Fuel Sloshing effect on Dynamic Loads

Jose Daniel Pérez Muñoz

June 19, 2014

Contents

Nomenclature

A/C	Aircraft
BEM	Boundary Element Method
CS	Certification Specification
DL	Doublet Lattice
DLM	Doublet Lattice Method
DTG	Discrete Tuned Gust
EAS	Equivalent AirSpeed
EASA	European Aviation Safety Agency
EMS	Engine Mounting System
FCS	Flight Control System
FEM	Finite Element Method
FVT	Flight Flutter Test (It is not named as FFT because that is usually referred to Fast Fourier Transform)
GVT	Ground Vibration Test
HTP	Horizontal Tail Plane
KEAS	Knots of Equivalent AirSpeed
M	Mach
MTOW	Maximum Take Off Weight
MZFW	Maximum Zero Fuel Weight
ODE	Ordinary Differential Equation
PDE	Partial Differential Equation

RF	Reserve Fuel
Solution 103 NASTRAN	Modal solution (Real eigenvalue analysis) http://es.scribd.com/doc/134539018/MSC-Nastran-2012-Dynamic-Analysis-User-s-Guide#page=58
Solution 112 NASTRAN	Modal Transient Response Analysis http://es.scribd.com/doc/134539018/MSC-Nastran-2012-Dynamic-Analysis-User-s-Guide#page=223
Solution 146 NASTRAN	Dynamic Aeroelastic Analysis http://es.scribd.com/doc/134539011/MSC-Nastran-Version-68-Aeroelastic-Analysis-User-s-Guide#page=75
SPH	Smoothed Particle Hydrodynamics
VDTG	Vertical Discrete Tuned Gust
VTP	Vertical Tail Plane

Acknowledgments

I would like to thank all the support from the Dynamics Department of Airbus Defence and Space and especially to:

- My tutor, Héctor Climent Mañez, who has worked very hard to prepare this project and who has helped me with all the questions I had. He had taught me Aeroelasticity in the University Carlos III and he made it so interesting that I requested to work with him, in his area of investigation, and in this specific project, in which we have both been excited. He has been a great support for me.

- Juan Tomás Viana Lozoya, who has been working in the department while I was there and taught me how to use Pam-Crash. Apart from his knowledge, I also appreciate his patience, since he was always willing to cooperate and help me.

- Sebastian Claverías Ceacero, who has been also working in the department while I was there and taught me the basics. He showed me how to deal with NASTRAN, other programs and how to work in a company like Airbus. He has also been very helpful and caring about the project.

I would like also to thank all the help and support from my university colleagues, especially to Santiago Casado Pérez, who has helped me throughout the degree and who has put up with me these four years.

And last, but not least, I thank all the support that my family has given me all these years.

Chapter 1

Motivation

1.1 Introduction

Aircraft wing up bending critical cases are obtained in the Discrete Tuned Gust (DTG) loads scenario. The simulation of this scenario needs accurate numerical models to represent the stiffness, mass distribution and unsteady aerodynamics of the aircraft.

There are many tests on ground (static test, Ground Vibration Test (GVT), ...) and inflight (Flight Flutter Test (FVT),...) that are used to validate these models.

There is another parameter that affects loads which has not received the same level of attention from academia, labs or industry; this parameter is **damping**. Current Airworthiness Regulations allow the use of 3% structural damping in lack of better values.

The critical mass configurations in DTG analysis are configurations with intermediate fuel contents. It is conjectured that if the fuel sloshing within the wing is taken into account, the amount of damping could be higher than 3% and then the total loads could be reduced, which in turn would decrease the wing structural weight and in a snowball effect this will improve aircraft performance and reduce fuel consumption and emissions.

Nowadays, the modeling methods of the aeronautical industry assume that the fuel mass is "frozen" and is attached to the tank moving with it. This modelization is not an accurate representation of the real behavior of liquids but it is conservative, leading to a slight penalty on weight. Although there are several programs that reproduce the performance of liquids, they are very computationally demanding to be used in the thousands of DTG cases required in industry.

The aim of this paper is to study how the effect of fuel sloshing can help to reduce the dynamic loads on the wing. The aircraft chosen for the study is the Airbus A400M military transport aircraft (Figure 1.1). Moreover, since the purpose is to understand in a better way the behavior of the aircraft, this paper could make the actual model (which is very precise) to be even more accurate in conditions with significant fuel movement compared with the real behavior.

Figure 1.1: Airbus A400M military transport aircraft.

Chapter 1 will demonstrate that the critical case for sizing of the wing is an intermediate fuel contents configuration and will prove that a higher damping helps to reduce dynamic loads. An estimation of the dynamic loads reduction is presented for the A400M case. This chapter also comments different ways to model the sloshing produced by liquids and how it has been treated in certain fields of industry.

In Chapter 2, a simplified model in NASTRAN is created to reproduce in a simpler way the behaviour of the wing. The main dynamic parameters of the wing (modal frequencies and modal shapes) have been used to create this model. Different variations and models are used in order to study the effect of fuel in dynamic loads.

Chapter 3 presents a virtual test and describes the model used in Pam-Crash, the SPH (Smoothed Particle Hydrodynamics) technique and how to apply it. SPH technique is an advanced tool for representing liquid behaviour and by which more accurate results could be obtained.

Chapter 4 covers the result of the virtual test applied to the Pam-Crash model. It includes the evolution of main parameters with the variation of fuel and ribs configurations.

Chapter 5 proposes how to relate Pam-Crash data with NASTRAN data through two ways. It also contains the expected benefits that this test could bring to the industry.

Chapter 6 proposes future work (improvements for the virtual test and a real physical test with its budget) and summarizes the steps followed.

1.2 Maths of dynamic response of the aircraft due to Discrete Gust

1.2.1 Basic assumptions

- **The analysis is linear.**
- **Implicit Finite Element Method (FEM) is used.**
- **The Discrete Tuned Gust (DTG) problem is solved in the modal base built with the normal modes of the structure.**
- **Motion assumptions** (needed for Doublet Lattice Method (DLM) equations).
  - Small motions (in order to make the analysis linear).
  - Harmonic motions (since this problem is only known in the frequency domain).
- **Structural model assumptions:**
  - The symmetric aircraft model is used (given by Airbus Group) since only frontal vertical discrete tuned gust (VDTG) is considered.
  - The normal modes are obtained from a model of the structure that makes use of the FEM technique (MSC/NASTRAN).
  - The structural model reproduces adequately the load path of the structure and the stiffness characteristics of the different aircraft components:
    - Lifting surfaces (wing, Horizontal Tail Plane (HTP), Vertical Tail Plane (VTP)...).
    - Engine and Engine Mounting System (EMS).
    - Fuselage.
  - The masses have been represented as lumped masses joined to strong points of the structure to avoid local undesirable modes.
  - The structural model is suitable to represent the dynamic behavior of the structure at least up to 50 Hz.

Figure 1.2: A400M Structural model.

- **Unsteady aerodynamics assumptions:**
  - Unsteady aerodynamics has been computed using the (DLM). The DL model (given by Airbus Group) includes flat panels to model lifting surfaces (wing, HTP and VTP) and control surfaces (Ailerons, Elevator, Rudder...).
  - The DL model mesh is suitable at least for modes up to 50 Hz.
  - The DL model is only valid for subsonic flow.
  - Structure-aerodynamic interpolation has been made by means of surface splines.
  - The unsteady aerodynamics is calculated for a range of reduced frequencies that covers the A/C response to atmospheric turbulence.

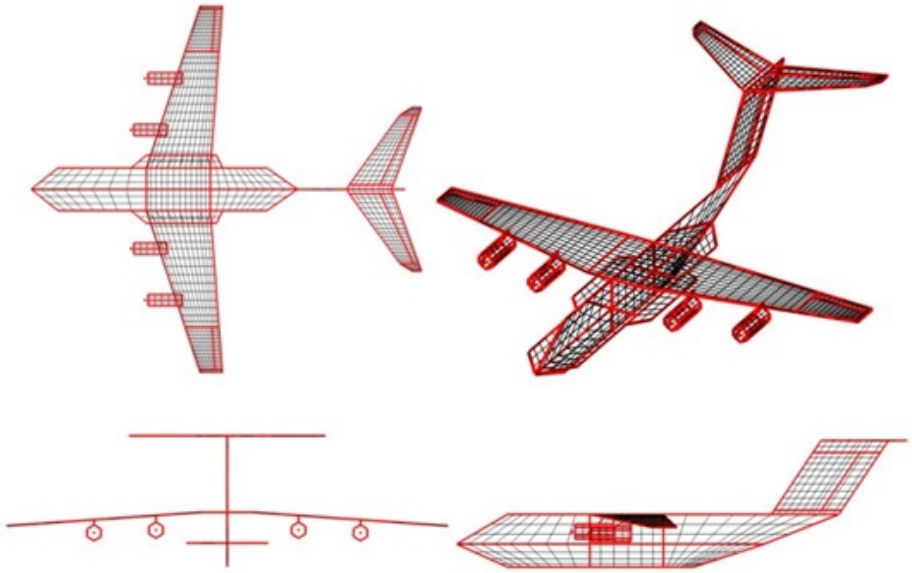

Figure 1.3: A400M Unsteady Aerodynamic model.

- **Flight Control System (FCS) model assumptions:**
  - FCS not considered.
- **Damping model:**
  - 3% viscous (Default)
- **Data recovery method:**
  - Summation of forces.
- **Total loads are obtained by summing up incremental (dynamic part) and 1g loads (Gravity & Steady-aerodynamics effects).**

1.2.2 Equations of motion

MSC/NASTRAN uses the following set of second order differential equations for the dynamic equilibrium of the system:

$$[M]\{\ddot{x}(t)\} + [B]\{\dot{x}(t)\} + [K]\{x(t)\} = \{F(t)\} \tag{1.1}$$

where the first term on the left hand side of the equation represents the inertia of the system (Mass matrix $[M]$ and acceleration of the points of the system $\{\ddot{x}(t)\}$), the second one is the force that the damping is trying to do in order to mitigate the

deformation (Damping matrix $[B]$ and velocity of the points of the system $\{\dot{x}(t)\}$), and the third one is the elastic force (Stiffness matrix $[K]$ and displacement of the points of the system $\{x(t)\}$). On the right hand side, the applied force is represented $\{F(t)\}$.

Equation 1.1 comes from the equilibrium of forces and moments at all points of the structure. The elements of $[M]$, $[B]$ and $[K]$ are assumed to be constants in MSC/NASTRAN making equation 1.1 linear.

Solutions of this equation are linear combinations of the free vibration modes of the structure. These modes can be obtained from a condensed form of Equation 1.1 in which $[B]$ and $\{F(t)\}$ are null. The remaining matrices are required to be symmetric. It is supposed that all parts of the system are vibrating sinusoidally with the same frequency,$f = \omega/2\pi$, and the same phase, i.e., that

$$\{x\} = \{\phi\}cos(\omega t) \tag{1.2}$$

where $\{\phi\}$ is a vector of real numbers and $cos(\omega t)$ is a scalar multiplier. Substituting 1.2 into the condensed form of 1.1 leads to the following expression:

$$[K - \omega^2 M]\{\phi\}cos(\omega t) = 0 \tag{1.3}$$

or

$$[K - \omega^2 M]\{\phi\} = 0 \tag{1.4}$$

since equation 1.3 must be valid at all instants of time. Nontrivial solutions exist only if the matrix $[K-\omega^2 M]$ is singular and this happens at a discrete set of frequencies, $f_i = \omega_i/2\pi$, called eigenfrequencies (modal or natural frequencies). For each frequency, there is a vector $\{\phi_i\}$ called eigenvector (or modal vector) that solves equation 1.4. Thus,

$$[K - \omega_i^2 M]\{\phi_i\} = 0 \qquad \text{for } i = 1, 2, 3..., N \text{ where } N \equiv \text{size of } [K] \text{ and } [M] \tag{1.5}$$

Each natural frequency and modal vector define a free vibration mode of the structure. In absence of damping and nonlinear effects, the structure can vibrate indefinitely at modal frequency f_i and with mode shape $\{\phi_i\}$.

The mode shapes found in this eigenvector analysis are used to relate the physical degrees of freedom $\{x(t)\}$ to a set of modal coordinates or generalized coordinates $\{\xi_i\}$ according to the following formula in matrix form

$$\{x\} = [\phi]\{\xi\} \tag{1.6}$$

where the i-th column of $[\phi]$ is $\{\phi_i\}$.

Until here, no approximation is made. However, a small approximation is introduced if only the modes with frequencies less than a cutoff frequency are included. The cutoff frequency should be at least twice the highest frequency which makes a significant contribution to the spectrum of the excitation. For most of the problems solved by FEM, the number of modes below the cutoff frequency is a small fraction of the total number of modes.

Now, plugging 1.6 into 1.1 results in n equations in m unknowns, where n is the number of physical degrees of freedom in $\{x\}$ and m is the number of modal coordinates in $\{\xi\}$. The number of equations is further reduced from n to m by pre-multiplying the whole equation times $[\phi]^T$ as can be seen in 1.7.

$$\underline{[\phi]^T[M][\phi]}\{\ddot{\xi}\} + [\phi]^T[B][\phi]\{\dot{\xi}\} + \underline{[\phi]^T[K][\phi]}\{\xi\} = [\phi]^T\{F(t)\} \tag{1.7}$$

if $[M]$ and $[K]$ have the same values as in equation 1.5, it can be shown that the underlined elements are diagonal because of the orthogonality properties of eigenvectors with respect to the mass and stiffness matrices. A similar orthogonality property cannot generally be found for the damping matrix $[B]$. However, it is frequently assumed (proportional damping) in order to achieve a diagonal modal damping matrix ($[\phi]^T[B][\phi]$). If this is assumed, each row of equation 1.7 becomes independent of the other rows. In order to obtain each of the modal coordinates, the following ordinary differential equation has to be solved:

$$m_i\ddot{\xi}_i(t) + b_i\dot{\xi}_i(t) + k_i\xi_i(t) = f_i(t) \tag{1.8}$$

or

$$\ddot{\xi}_i(t) + 2\zeta_i\omega_i\dot{\xi}_i(t) + \omega_i^2\xi_i(t) = \frac{1}{m_i}f_i(t) \tag{1.9}$$

where $\zeta_i = b_i/(2m_i\omega_i)$ is the modal damping ratio, and $\omega_i = \sqrt{k_i/m_i}$ is the modal frequency.

MSC/NASTRAN solves the equation when the mass matrix, stiffness matrix and damping matrix are defined from the structural model (mass and stiffness) and from the input of the program (damping).There are two types of damping: viscous damping (which is the usual one) and structural damping. The first one is proportional to velocity and the second one, to displacement. Assuming harmonic oscillation, viscous damping is equal to half the structural damping ($\zeta = g/2$). Reference value in this report is viscous damping of 3%. This percentage is the ratio of the damping over the critical damping that the structure has to have to produce no oscillations.

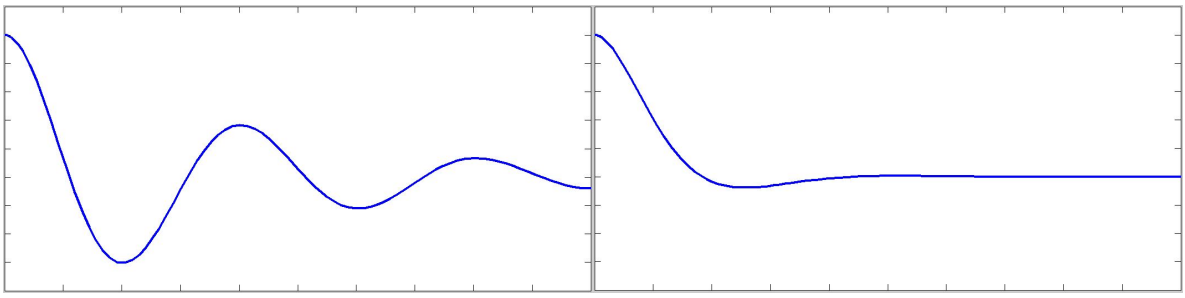

Figure 1.4: Underdamped movement (left) and critically stable movement (right).

The main task is to increase that value by considering fuel sloshing and JUSTIFY that change by the study presented in this paper.

1.3 Critical case

The first thing to do is to identify which is the most critical case of up bending. This is done with the different mass states of the aircraft. The following mass states have been considered:

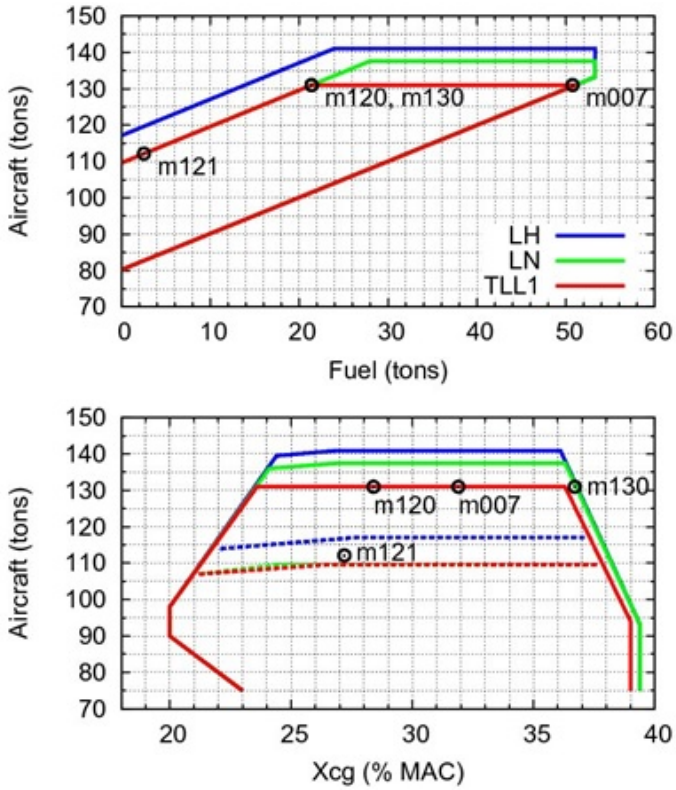

Figure 1.5: Mass states of A400M. TLL1, LH and LN are configurations of the A400M which are not relevant for the study.

M121 corresponds to a state where only reserve fuel is inside the aircraft and payload is maximum, this is commonly known as Maximum Zero Fuel Weight plus Reserve Fuel (MZFW+RF). M120 and M130 are two states where the aircraft has the same mass but it is distributed so that the center of gravity is forward (M120) or rearward (M130). These two states are known as Maximum Take-Off Weight (MTOW) with maximum payload. The last point studied is the M007, which is the point where no payload is admitted and the fuel is maximum, it is known as MTOW full fuel.

The aircraft is flying at sea level, at $300 knots$ and $M = 0.72$.

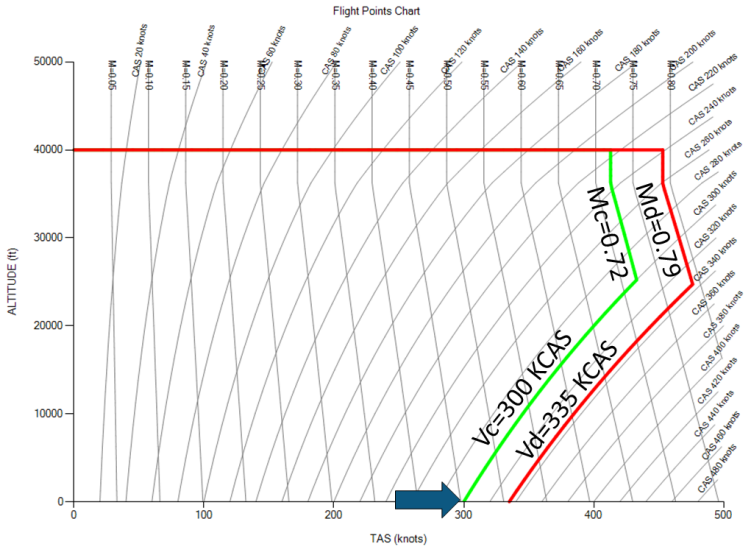

Figure 1.6: A400M flight envelope.

The sizing case for the wing structure is the vertical gust encounter. This gust produces an increase of lift that generates a moment at the root of the wing, which is the largest one from all possible scenarios of the aircraft. Since the aircraft is going to be exposed to the gust at $300 KEAS$ (Knots EAS) at sea level the following gust profiles are studied:

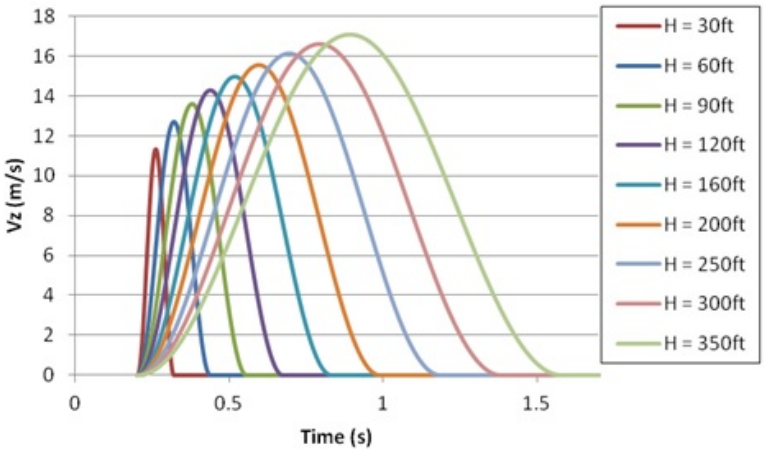

Figure 1.7: Different gust profiles at 300 KEAS.

These profiles are the ones that follow the EASA CS 25.341 rule which provides the following formula:

$$\begin{cases} U = \frac{U_{ds}}{2}\left(1 - cos\left(\frac{\pi s}{H}\right)\right) & \text{for } 0 \leq s \leq 2H \\ 0 & \text{for } s > 2H \end{cases} \tag{1.10}$$

where $U_{ds} = U_{ref} F_g (H/350)^{1/6}$, H is the gust gradient, which is the distance parallel to the aircraft flight path for the gust to reach its peak velocity, s is the distance penetrated into the aircraft, F_g is the alleviation factor (which is 1 for tactical missions), and U_{ref} is the design gust velocity, which has to be linearly reduced from $56 ft/s$ Equivalent AirSpeed (EAS) at sea level to $44 ft/s$ at $15000 ft$. Since the study is at sea level, the reference gust velocity is fixed at $56 ft/s$.

The sizing magnitude for the structure of the root of the wing is the upward bending moment, so the time history of this magnitude is shown in Figures 1.8, 1.9, 1.10 and 1.11, normalized to reach a 100% value at the maximum bending moment among all the cases. The response of the aircraft has been found using MSC/NASTRAN (solution 146) and the solution post-process has been done using an in-house Airbus Defence & Space program developed by the Dynamic department called DYNLOAD. Then, it has been graphically represented with the program GNUPLOT.

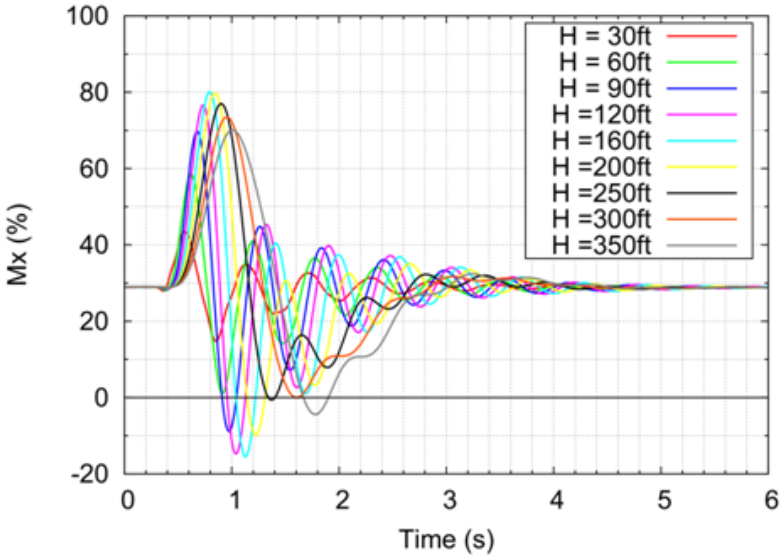

Figure 1.8: MTOW full fuel UP Bending Moment at Wing root.

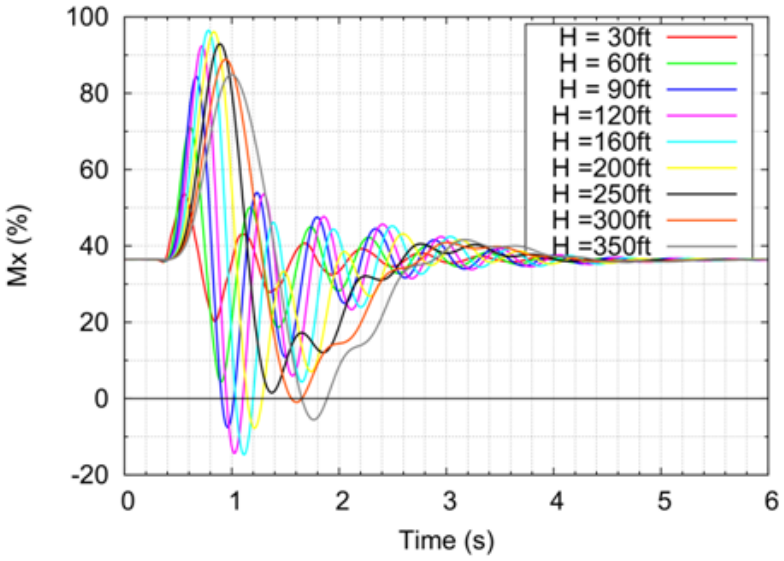

Figure 1.9: MTOW max. payload (forward c.g.) UP Bending Moment at Wing root.

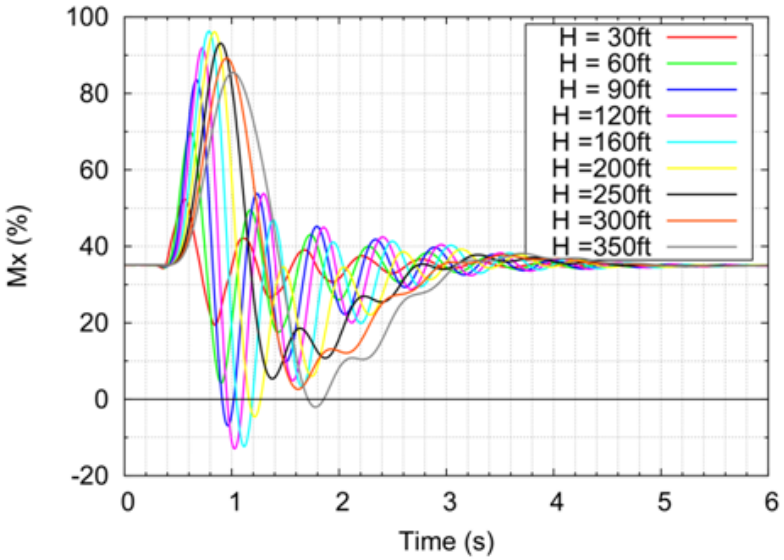

Figure 1.10: MTOW max. payload (rear c.g.) UP Bending Moment at Wing root.

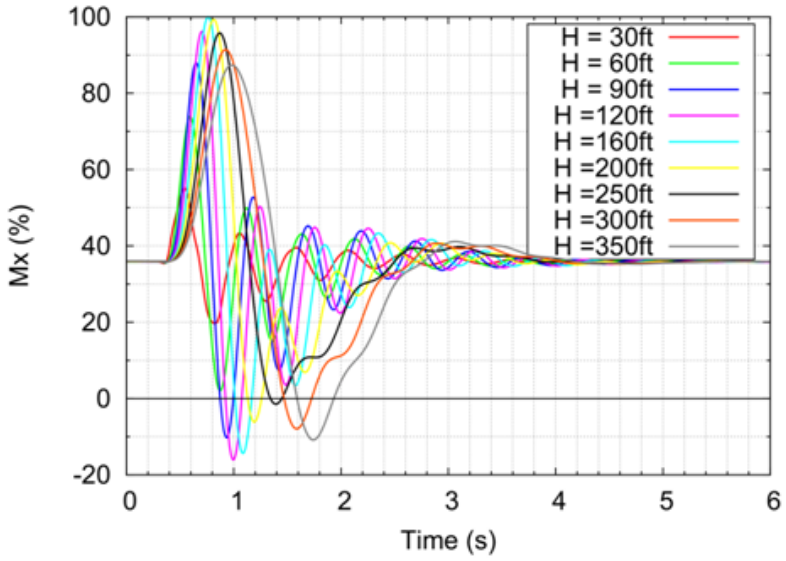

Figure 1.11: MZFW with reserve fuel UP Bending Moment at Wing root.

The highest peak is reached in all cases with the gust that is $H = 160ft$ long. This is because the content of frequency of the gust is exciting the first bending mode of the wing. It can be appreciated that the bending moment is not 0 before the gust is found but a certain value (the gust is set to reach the aircraft $0.2s$ from the beginning of the simulation). That is the effect of static 1-g loads. Given that the aircraft has weight, the wing has to produce lift enough to sustain the aircraft in the air, this upward force deform the wing and bends it, producing a static value of the moment at the root.

The numerical values of percentages of the shear force, bending moment and torsion moment are presented in the next table:

Mass state	Shear Force at the root		Bending moment at the root (positive up bending)		Torsional moment at the root (positive pitch up)	
	Max. value	Critical gust	Max. value	Critical gust	Max. value	Critical gust
MTOW full fuel	(59.3%)	H = 200ft	(80.1%)	H = 160ft	(78.2%)	H = 90ft
MTOW max payload (forward cg)	(88.9%)		(96.4%)		(89.1%)	
MTOW max payload (rear cg)	(88.7%)		(96.2%)		(89.7%)	
MZFW with reserve fuel	(100%)		(100%)		(100%)	H = 60ft

Table 1.1: Peak values from gust analysis.

Although the critical value for Shear force comes from a different gust length, the

magnitude that sizes the wing is the Bending moment at the root, so only the $160ft$ gust will be studied.

From now on, the cases of MZFW with reserve fuel and MTOW max payload with forward cg are studied in view of the fact that those lead to the highest values for the bending moment found from the analysis. The MTOW full fuel case has been dropped from the analysis because the peak values were lower than the other cases and also because if the tank is full of fuel, its behavior is very similar to a rigid body, so no remarkable fuel sloshing effect will be present.

1.4 Sensitivity to damping

The next step is to show how the aircraft would respond if the damping coefficients are changed. For this task, the damping input in MSC/NASTRAN is varied in the range of 1% to 10% and the results were the following:

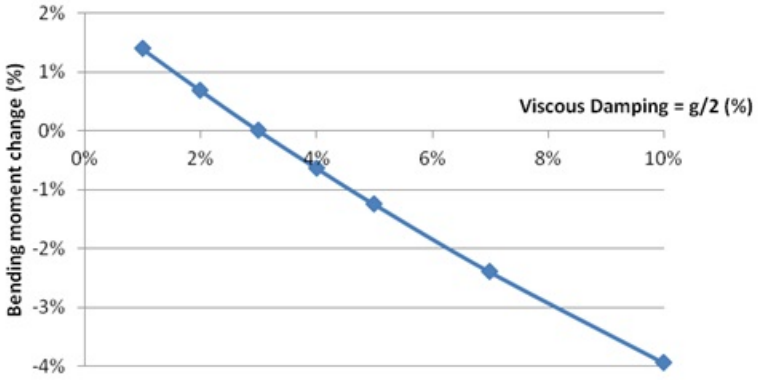

Figure 1.12: Variation of (+) Peak Bending moment with viscous damping for MTOW max. payload (forward cg) for a H=160ft gust.

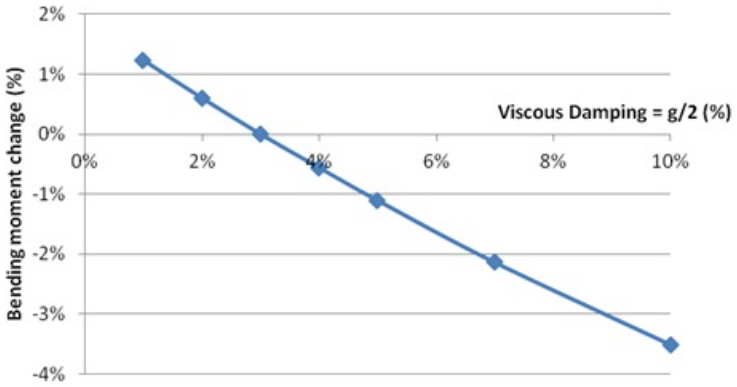

Figure 1.13: Variation of (+) Peak Bending moment with viscous damping for MZFW with reserve fuel for a H=160ft gust.

The graphs shown are in terms of the percentual difference of moment with respect to the nominal damping, 3%. As can be seen, the increase of damping ratio reduces the bending moment; for example, a reduction of 3.5% of bending moment can be achieved with a viscous damping of 10%.

The numerical values of percentages of the maximum shear force, bending and torsional moment reduction are exposed in Table 1.2 for MTOW with forward cg and in Table 1.3 for MZFW:

Viscous Damping = g/2	Max. Peak Shear force	Max. Peak Bending moment	Min. Peak Torsional moment
	%	%	%
1%	0,78	1,39	0,41
2%	0,38	0,68	0,20
3%	0,00	0,00	0,00
4%	-0,34	-0,63	-0,20
5%	-0,68	-1,25	-0,39
7%	-1,29	-2,40	-0,77
10%	-2,08	-3,95	-1,32

Table 1.2: MTOW max. payload (forward cg) study for a H=160ft gust varying the damping.

Viscous Damping = g/2	Max. Peak Shear force	Max. Peak Bending moment	Min. Peak Torsional moment
	%	%	%
1%	0,67	1,23	0,34
2%	0,33	0,60	0,17
3%	0,00	0,00	0,00
4%	-0,29	-0,56	-0,16
5%	-0,59	-1,11	-0,31
7%	-1,12	-2,14	-0,60
10%	-1,82	-3,51	-1,00

Table 1.3: MZFW with reserve fuel study for a H=160ft gust varying the damping.

If a 5% of viscous damping is justified with the fuel sloshing, more than 1% of the bending moment is reduced. This reduction on bending moment would reduce the mass of the wing structure around 65kg (i.e. 130kg in the case of the A400M).

1.5 Introduction and literature survey in fuel sloshing

Sloshing is referred to the movement of liquid that is inside of another object. This liquid that sloshes can interact with the container object in order to change its dynamic behaviour.

This effect is especially important in spacecraft tanks and rockets. It is also known that partially filled tanks affect the dynamics of manned aircrafts and missiles.

There is an extensive literature that has studied the effect of liquid sloshing in tanks.

In [1] ([#] stands for the identification number in Bibliography), the effect of small fluid oscillations are studied with the Boundary Element Method (BEM).

In [2] and [3], different ways of modelization of the fluid are described. These modelizations are assume also for small fluid oscillations. Although [2] is a very complete study of liquid movement, [3] is more focused on the effects that this movement produces on aerospacial tank structures. The two ways of modelization that have influenced this work the most are the pendulum and the springs ones.

Both of them are built as a "fixed mass" and an "effective mass" as can be seen in Figure 1.14. The fixed mass acts as a solid that is attached to the tank in both of the cases and the effective mass is moving with respect to the tank, but the connections are different in either case.

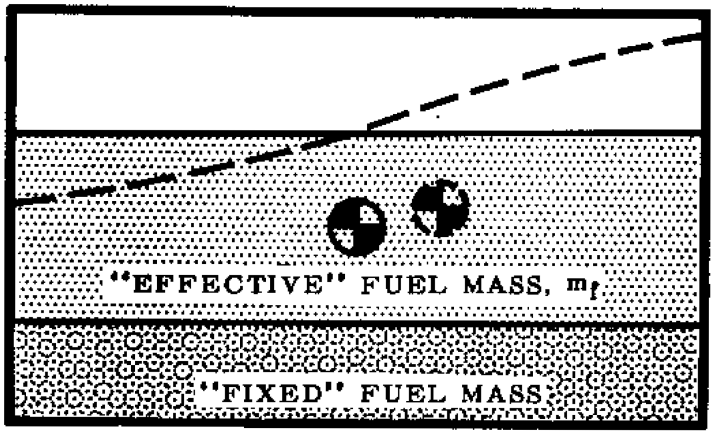

Figure 1.14: Fixed and effective masses representation (Source: [3]).

For the first modelization, a solid bar connects the effective mass to the fixed one and moves as a pendulum. This modelization was studied to be implemented in the model of Chapter 2, but the fact that gravity will not be used led to the rejection of this way (gravity is not considered because it has a negligible effect during the short time of a dynamic test). On the other hand, the second modelization (Figure 1.15) consists in several effective masses that are connected to the tank structure by a spring in one side and a damper in the other side. This modelization was more attractive because gravity is not present. However, linear freedom of the masses was not desired since greater displacements could make the fuel move in two or three axes.

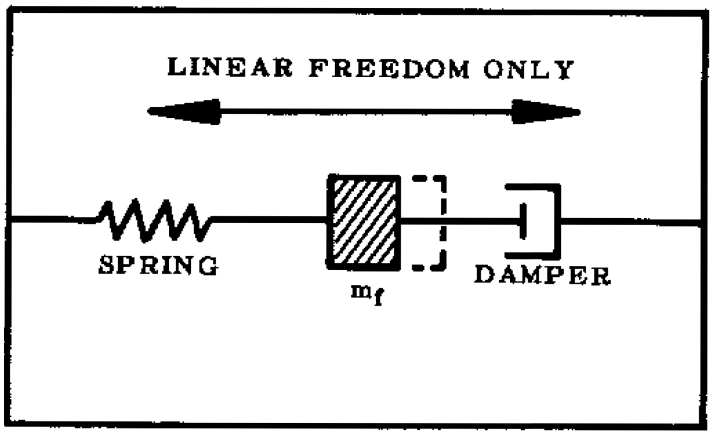

Figure 1.15: Single degree of freedom analog to sloshing fuel (Source: [3]).

A pendulum modelization is studied in depth in [4], where it is proved that it is very precise for a spherical vessel and was tested in a physical experiment and in a code in MatLab. It also proved that intermediate liquid contents are more prone to slosh as can be seen in Table 1.4.

Fill level	10%	20%	30%	40%	50%	60%	70%	80%	90%	99%
Fixed Mass (kg)	0.008	0.064	0.209	0.476	0.890	1.456	2.161	2.965	3.783	4.356
Effective Mass (kg)	0.114	0.392	0.738	1.068	1.303	1.386	1.277	0.964	0.479	0.028

Table 1.4: Mass distribution for 8" sphere using pendulum modelization (Source: [4]).

Another way to reproduce the fluid behaviour is through SPH technique, which is explained in Section 3.2.

In [5], the equations of this technique are described along with its applications in thermodynamics, impacts and astrophysics.

Airbus has studied this phenomenon through SPH technique too, [6] studies the effect of fuel sloshing in the pressure that is applied onto the skin of the walls of a rectangular tank. It also covers the variation of the center of gravity of the system.

Recently, [7] was presented by Airbus where the content of this study (fuel sloshing), bird splitting and ditching loads are treated with SPH technique.

Chapter 2

Proof of concept

2.1 Introduction

The intention of this chapter is to:

- Create a simple model that reproduces the main dynamic characteristics of the wing (Section 2.2).
- Demonstrate that intermediate fuel contents are the most critical cases (Section 2.3).
- Use an alternate model which considers that fuel masses can move by means of springs (Section 2.4). This model would represent a more realistic behaviour of the fuel.

In Sections 2.5 and 2.6, a correlation between the springs model and damping is treated.

2.2 Model

A simplified model is proposed to perform all the analysis in this project. The intention is that the model should reproduce the first wing bending mode in terms of frequency and mode shape of the A400M wing. Due to this "dynamic similarity" the conclusions obtained with this model could be applied to the real aircraft.

In addition, it is intended that the model represents "an easy physical reality" in such a way that it could be easy for the engineer to extract conclusions and "physical insight" from the results of the numerical simulations.

The model will represent a straight rectangular wing of $10m$ span, clamped at the wing root. The wing section will be also rectangular. The origin of coordinates is placed as can be seen on Figure 2.1 and its section is represented in Figure 2.2.

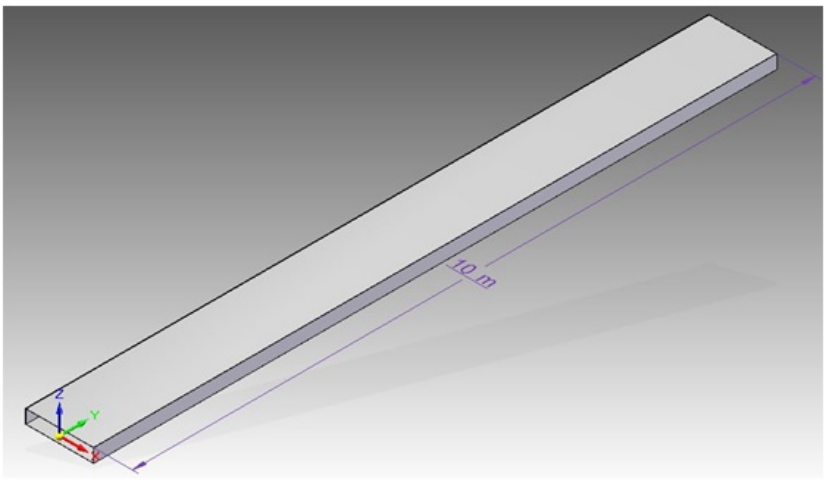

Figure 2.1: 3D view of the model and origin of coordinates.

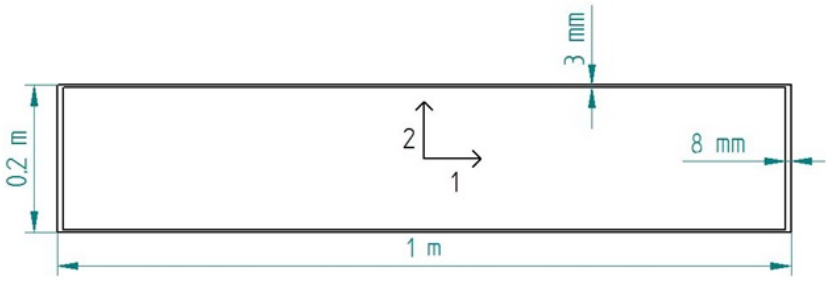

Figure 2.2: Model section.

The beam has the following properties:

- $I_1 = 1.26{\cdot}10^{-3}m^4$
- $I_2 = 6.8{\cdot}10^{-5}m^4$
- $I_{12} = 0m^4$
- $J = 2.23{\cdot}10^{-4}m^4$
- $Area(A) = 9.1{\cdot}10^{-3}m^2$
- $Mass(m) = 245.8Kg$

The material used has the following properties:

- $Young's\ \ modulus(E) = 72GPa$

- $Poisson's\ ratio(\nu) = 0.33$
- $Density(\rho) = 2700Kg/m^3$

This model is represented in MSC/NASTRAN as can be seen in Figure 2.3:

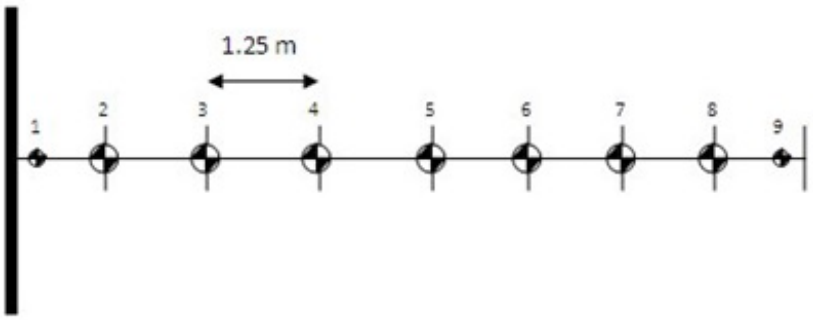

Figure 2.3: MSC/NASTRAN stick model representing grids (vertical lines) and lumped masses (circles).

The characteristics of the masses are presented in Table 2.1. These masses have been placed with the entry CONM2 of NASTRAN and they have been assigned to the grids (dots in Figure 2.3). Each grid is connected to the adjacent ones by the CBEAM entry.

	Mass (kg)	Ixx (kg m²)	Iyy (kg m²)	Izz (kg m²)
Small dots (1,9)	15.4	0.6	2.2	2.6
Big dots (2 though 8)	30.7	4.2	4.5	8.3

Table 2.1: Masses characteristics.

Once the model is defined, the next thing to do is to proof that this beam would represent the wing behavior. For the clamped beam with constant section, there is an analytical solution for the bending modes frequencies. The PDE that describes the motion of the beam is the following[1]:

$$\rho A \partial_{tt} w(y,t) = -EI\partial_{yyyy} w(y,t) + f(y,t) \tag{2.1}$$

[1]NOTE: The study is made in abscence of gravity.

where the subscript for ∂ indicates the derivative with respect to time (t) or longitudinal position of the beam (y), w is the vertical displacement of a point of the continuous beam, E is the Young's modulus, I is the cross section moment of inertia with respect to the rotating axis and f is the external force, which is 0 in order to obtain the modal frequencies. The boundary conditions for a clamped-free beam are the following:

$$\begin{cases} w(0,t) = 0 & \text{no displacement at root} \\ \partial_y w(0,t) = 0 & \text{no rotation at root} \\ \partial_{yy} w(L,t) = 0 & \text{no torque at end} \\ EI\partial_{yyy} w(L,t) = 0 & \text{no shear at end} \end{cases}$$

Equation 2.1 is solved using separation of variables, this is, assuming $w(y,t) = Y(y)T(t)$. Then, equation 2.2 is obtained. It is possible to show that a non-zero negative constant ($-\sigma^2$) is necessary to have an oscillatory response.

$$\frac{\partial_{tt} T}{T} = -\frac{EI}{\rho A}\frac{\partial_{yyyy} Y}{Y} = -\sigma^2 \tag{2.2}$$

Equation 2.2 is recasted as two ODEs:

$$\partial_{yyyy} Y - \sigma^2 \frac{\rho A}{EI} Y = 0 \tag{2.3}$$

$$\partial_{tt} T + \sigma^2 T = 0 \tag{2.4}$$

The solution for 2.3 is the implicit equation 2.5:

$$cos(\beta_n L) cosh(\beta_n L) = -1 \tag{2.5}$$

where $\beta_n^4 = \sigma_n^2 \frac{\rho A}{EI}$. The solution for this equation is $\beta_1 L = 1.8751, \beta_2 L = 4.6941, \beta_3 L = 7.8548....$ Since the intention is to reproduce the first bending mode, $\beta_1 L$ is used. From equation 2.4, it is possible to show that the frequency of the system is $f_n = \sigma_n / 2\pi$ which leads to the frequency equation of the first bending mode:

$$f_1 = \frac{(\beta_1 L)^2}{2\pi L^2}\sqrt{\frac{EI}{\rho A}} = 2.49656 Hz \tag{2.6}$$

This value is almost exact compared with the one that the solution 103 in MSC/NASTRAN computes, which is $2.49735 Hz$. These values are very similar to that of the first bending mode of the A400M wing (around $2.5 Hz$).

2.3 Normal modes sensitivity to fuel content

The model is filled as if the fuel were a solid mass ("frozen" fuel from now on) attached to the structure. The fuel has a density of $840Kg/m^3$. The fuel mass has been distributed among the dots of Figure 2.3.

Solution 103 is run for different fuel quantities and the evolution of frequency of the first wing bending is shown in Figure 2.4.

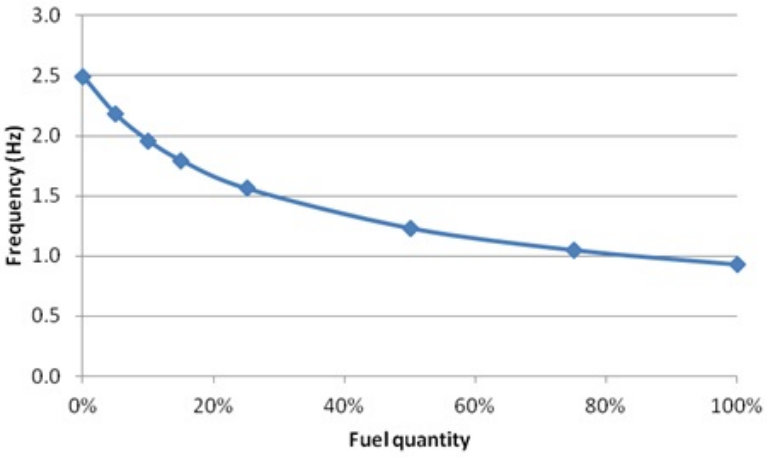

Figure 2.4: Evolution of 1^{st} wing bending frequency for different fuel quantities.

As expected, when the mass of a system is increased, the natural frequency of it decreases. When the stiffness of a system is increased, the natural frequency increases.

2.3.1 Transient excitation

The model is loaded with a transient vertical force at the tip (Figure 2.5)

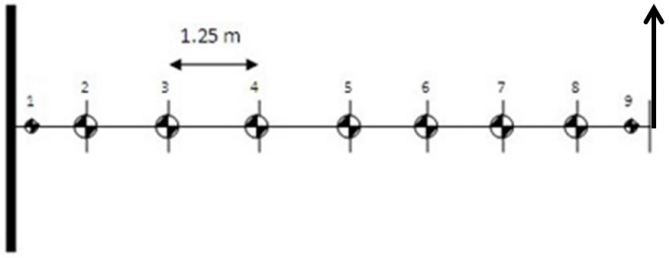

Figure 2.5: Set up.

This load has a $1 - cos$ shape (Figure 2.6) and its frequency content is similar to the $H = 160ft$ gust at $300KEAS$. It has a value of $1KN$ at its peak value.

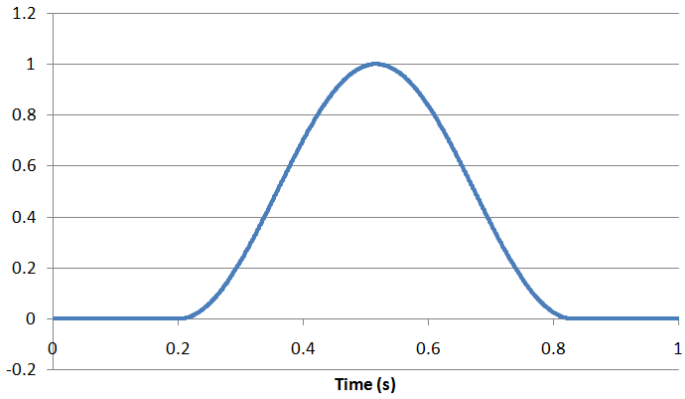

Figure 2.6: Transient force shape.

The dynamic response of the model has been extracted with solution 112 in MSC/NASTRAN. The analysis has been repeated for all fuel contents in the beam.

The peak bending moment at the root of the beam is presented in the next figure as a function of the fuel quantity.

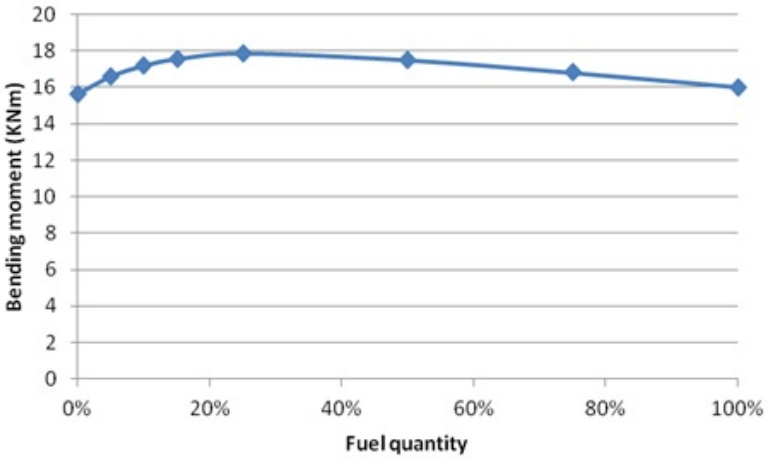

Figure 2.7: Evolution of peak bending moment with respect to the fuel quantity.

Figure 2.7 shows that the bending moment has a maximum around 25% of fuel quantity. The reason is that the $1-cos$ load is exciting the first bending mode frequency (around $1.6Hz$) for that particular fuel content. The numerical values are presented in the following table.

Fuel quantity (%)	Fuel quantity (kg)	f(Hz)	Max. Acceleration at the tip (m/s2)	Max. Displacement at the tip (m)	Max. Shear force (KN)	Max. Bending moment (KNm)
0%	0	2.50	9.43	0.100	1.97	15.62
5%	77	2.18	11.09	0.105	2.13	16.59
10%	153	1.96	11.18	0.107	2.23	17.19
15%	230	1.80	10.52	0.109	2.30	17.55
25%	384	1.56	8.71	0.109	2.37	17.87
50%	767	1.23	5.63	0.105	2.29	17.49
75%	1151	1.05	3.85	0.099	2.27	16.79
100%	1535	0.93	2.94	0.093	2.22	16.00

Table 2.2: Sensitivity to fuel quantity data.

Once the critical case has been identified, the 25% fuel quantity case is going to be studied for a different model of the fuel connection to the wing in Section 2.4. This is a model in which the fuel masses are not rigid masses that follow the beam but are connected with a spring.

2.4 Sensitivity to fuel-to-structure connection stiffness

The model of this section has been modified linking masses by springs to the grids of the structure. The way to do this in NASTRAN is to create new grids and superpose them on the existent grids. Then, the mass of the fuel is assigned to each new grid with CONM2 and finally, the new grid is connected by a spring to the structural grid with the entry CELAS2 (Figure 2.8). This is done for the 6 degrees of freedom (translation and rotation in x, y and z axes).

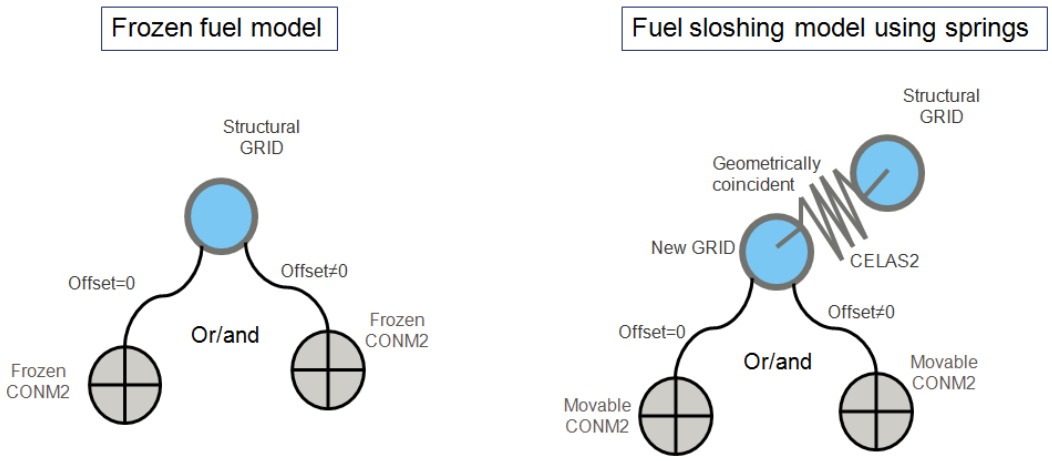

Figure 2.8: Connection between different elements.

All springs have the same stiffness. The mass of fuel is the one corresponding to 25% of the fuel quantity.

A sensitivity analysis of the evolution of the first bending mode frequency with respect to the spring stiffness has been performed. The frequency of the first bending mode has been computed with respect to the stiffness of the springs. When introducing masses attached with springs, new modes appear (fuel modes) and these modes have to be differentiated with respect to the modes of the beam.

Figure 2.9 shows that two different modes are to be considered regarding the bending mode of the structure:

1. Fuel mass and beam move in phase. This mode is similar to the "frozen" fuel mode, where the masses follow the movement of the structure.

2. Fuel mass and beam move out of phase. In this mode, the fuel masses move in opposite direction to the structure masses leading to a compensation of inertia.

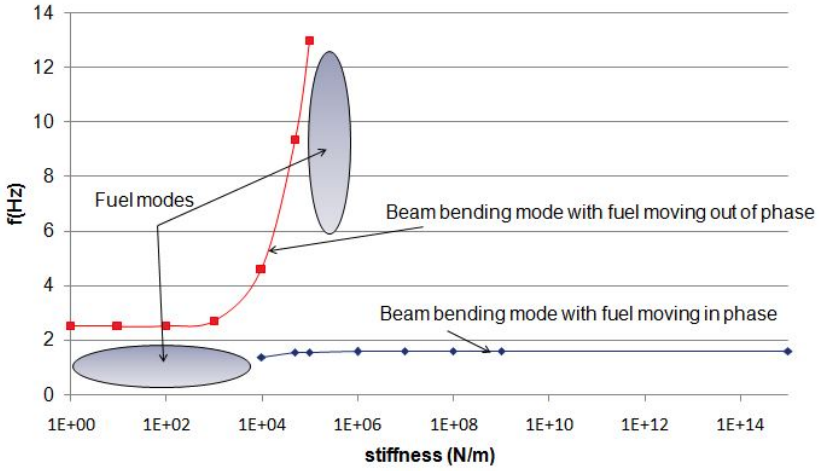

Figure 2.9: Evolution of bending mode with stiffness.

If the stiffness is further reduced, the springs start to behave as if there were no link between fuel and structure making fuel masses remain at the initial position. When this is achieved, the results make no sense because the system is behaving as an empty beam (fuel is no longer interacting with the beam and frequency tends to $2.5Hz$).

2.4.1 Transient excitation

Applying the same transient load of Section 2.3.1 varying the stiffness, the evolution of loads is the following:

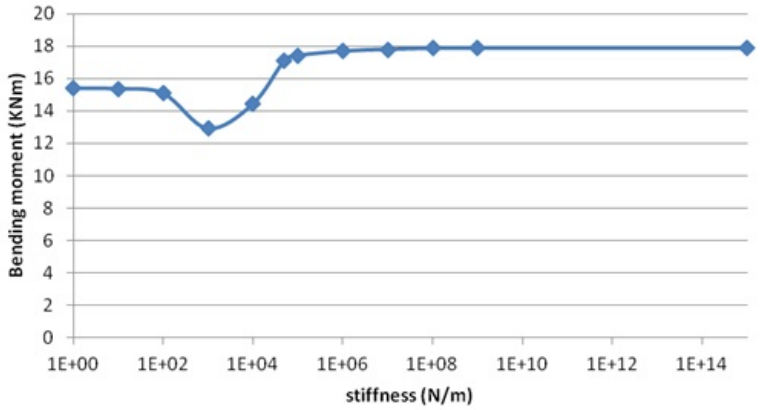

Figure 2.10: Peak bending moment evolution for different stiffness.

In Figure 2.10 is shown how the bending moment is reduced when stiffness is reduced (for values lower than $1{\cdot}10^4 N/m$ the results are not considered reliable because fuel

modes are acting in a non-physical way, i.e. the displacement of the fuel masses exceeds the width of the fuel tank, or the fuel masses do not move).

The conclusion of this study is that movable fuel masses may reduce dynamic loads with respect to frozen fuel.

A table with the numerical value of the peak bending moment among other data is showed below:

Stiffness (N/m)	Max. Acceleration at the tip (m/s2)	Max. Displacement at the tip (m)	Max. Shear force at the root (KN)	Max. Bending moment at the root (KNm)
1E+15	8.71	0.109	2.37	17.87
1E+09	8.71	0.109	2.37	17.87
1E+08	8.71	0.109	2.37	17.87
1E+07	8.71	0.109	2.36	17.86
1E+06	8.68	0.109	2.25	17.79
1E+05	8.41	0.107	2.16	17.68
5E+04	8.00	0.105	2.12	17.40
1E+04	5.44	0.090	2.09	17.09
1E+03	6.16	0.085	1.75	14.42
1E+02	9.13	0.098	1.28	12.91
1E+01	9.40	0.099	1.58	15.08
1E+00	9.42	0.100	1.62	15.36

Table 2.3: Sensitivity to stiffness data

The study of better ways to simulate the behavior of the fluid is presented in next chapter, where a model of the beam in Pam-Crash is built. This software represents the fluid particles and the movement of them.

2.5 Sensitivity to damping

This section shows sensitivity of tip response and root loads to damping. Viscous damping has been varied from 1% to 10% (NOTE: 3% was the nominal value used in previous section).

The fuel content selected for this sensitivity analysis has been set in 25%.

Since mass and stiffness of the whole system remain unchanged, the normal modes of the beam-fuel system remains the same.

As expected, the root loads decrease when increasing damping. Figure 2.11 shows the evolution of bending moment with damping.

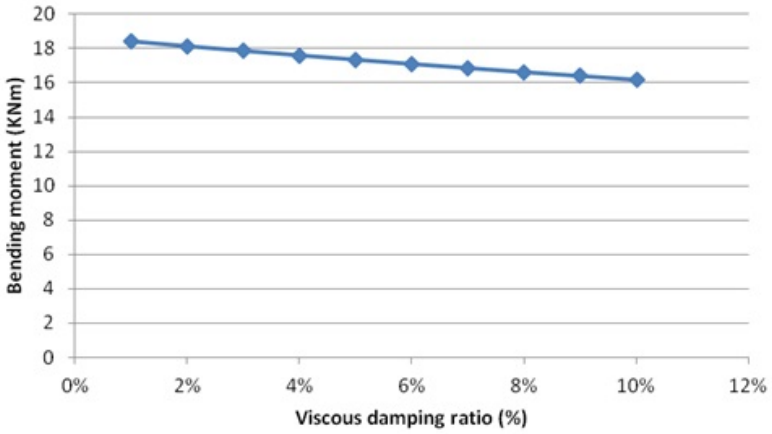

Figure 2.11: Peak bending moment with respect to the damping of the system.

Although values lower than 3% are not desirable and higher than 8% may not be realistic, they help to visualize how the damping ratio affects root loads. The next table contains the numerical values of the most interesting parameters for this model.

Damping (%)	Max. Acceleration at the tip (m/s2)	Max. Displacement at the tip (m)	Max. Shear force at the root (KN)	Max. Bending moment at the root (KNm)
1%	9.54	0.112	2.45	18.41
2%	9.11	0.111	2.41	18.13
3%	8.71	0.109	2.37	17.87
4%	8.33	0.108	2.34	17.61
5%	7.97	0.106	2.30	17.36
6%	7.62	0.105	2.27	17.11
7%	7.30	0.103	2.23	16.88
8%	7.00	0.102	2.20	16.65
9%	6.72	0.101	2.17	16.42
10%	6.45	0.100	2.14	16.21

Table 2.4: Sensitivity to damping data.

2.6 Correlation between spring stiffness of the fuel-to-structure connection and damping

From the two previous sections, a correlation can be extracted between the equivalent damping and the fuel-to-structure stiffness that produce the same peak bending moment at the beam root.

Since the system starts to behave as if it has no fuel for values of the stiffness less than $1{\cdot}10^4 N/m$, the correlation has been made for values higher than $5{\cdot}10^4 N/m$ and the results were the following for the bending moment:

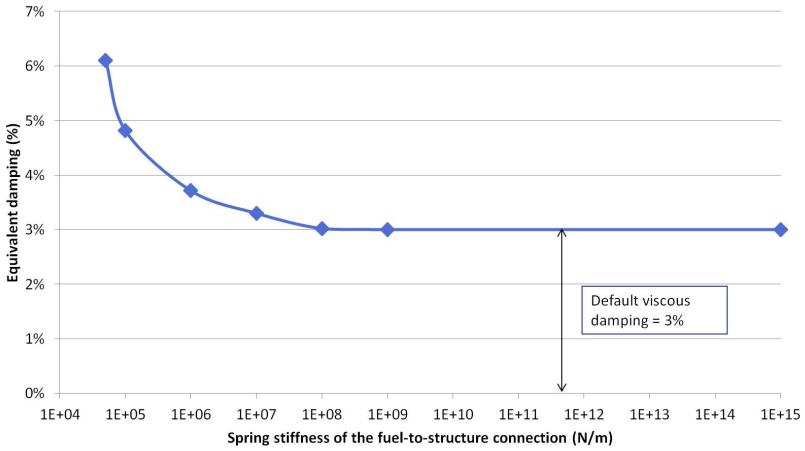

Figure 2.12: Bending moment correlation between Stiffness and Damping.

Other interesting magnitudes are presented in Figure 2.13 and the numerical values are listed in Table 2.5.

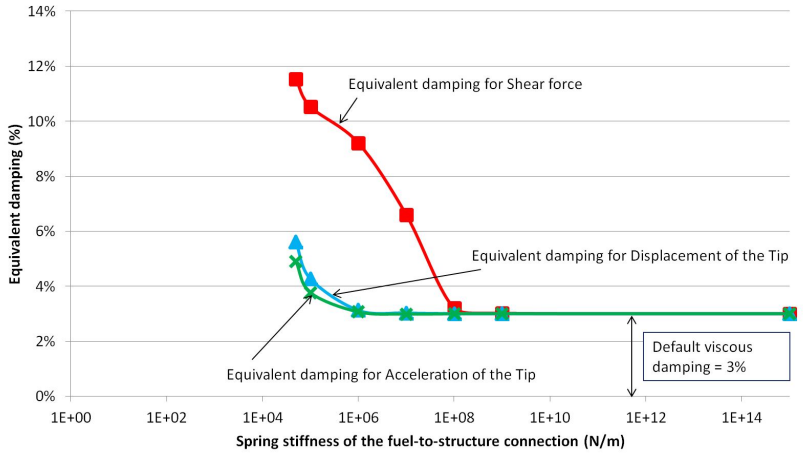

Figure 2.13: Correlation between Stiffness and Damping for several magnitudes.

Stiffness (N/m)	Equivalent damping for Bending moment	Equivalent damping for Shear force	Equivalent damping for Displacement of the tip	Equivalent damping for Acceleration of the tip
1E+15	3.00%	3.00%	3.00%	3.00%
1E+09	3.00%	3.02%	3.00%	3.00%
1E+08	3.02%	3.21%	3.00%	3.00%
1E+07	3.30%	6.60%	3.03%	2.99%
1E+06	3.71%	9.21%	3.12%	3.07%
1E+05	4.81%	10.53%	4.27%	3.77%
5E+04	6.11%	11.53%	5.60%	4.90%

Table 2.5: Correlation Stiffness-Damping data.

2.7 Conclusion of the proof of concept

This chapter has shown:

- A simplified modeling of fuel sloshing (like a spring to simulate fuel-to-structure connection).
- For certain values of this fuel-sloshing-spring, there is a reduction of loads with respect to frozen-fuel like loads.
- A correlation between fuel-sloshing-spring and global damping is feasible.

This is the proof of concept that a proper consideration of fuel sloshing may result in a dynamic loads reduction and, in turn, a structural weight reduction.

This concept will be further developed in the subsequent chapters of this report.

Chapter 3

Design of the fuel sloshing virtual test

3.1 Introduction

The methodology selected for designing a fuel sloshing virtual test has been a numerical simulation using EXPLICIT FEM technique in which the fuel contents have been simulated using SPH particles (Smooth Particle Hydrodynamics).

In Section 3.2, the SPH technique is presented. This technique will be used to model the internal fuel in a better way than with springs.

In Section 3.3, the explicit FEM technique is compared with implicit technique used in Chapters 1 and 2. The advantages and disadvantages of these methods are discussed.

Finally, in Section 3.4, the description of the virtual test and the models used are commented. This section also covers the method to identify the extra damping that the fuel adds to the structure.

In this chapter, the program Pam-Crash was used since it can work with SPH technique.

3.2 Introduction to SPHs

SPH particles will be used in this study to model the particles of the internal fuel.

SPH was invented to simulate non-axisymmetric phenomena in astrophysics. This method is easy to work with and gives reasonable accuracy.

The SPH method is a particle method and it does not need a grid to calculate spatial derivatives. Instead, they are found by analytical differentiation of interpolation formulae. Equations of momentum and energy become sets of ordinary differential equations which are easy to understand in mechanical and thermodynamical terms. However, SPH method cannot handle complex physics in three dimensions with the same ease. That is another reason why the model of a simple cantilever beam was selected. Equations and behaviour of SPHs are described in [5].

SPH particles have to be defined with different parameters in Pam-Crash:

- Volume that the particles occupy. The volume chosen for this project was the equivalent to a $2.5cm$ side cube ($1.5625 \times 10^{-5} m^3$), which results in a sphere of $1.55cm$ of diameter. Smaller SPH particles were tested and the precision was the same and the step time is increased.

- Density. In order to reproduce a real physical test, water is used since it is a very safe liquid and easy to obtain. Then, density was set to $1000 Kg/m^3$.

- Contact distance. Although the SPH particles share information between them and know when they are in the influence field of another particle, the distance that is required to contact with the structural model has to be an input data. For the case of the $20mm$ model, the contact distance was set to $10.2mm$.

- Contact surfaces. SPH particles need to know which are the surfaces they have to contact with. This will be particularly useful in Sections 4.2 and 4.2.1.

- Compression contact. When SPH particles are subjected to high or low forces due to other SPHs or to the structure, there is an option to decrease or increase the contact distance to simulate the compression and expansion. This parameter was set to 90% of the contact distance for compression and 140% for the expansion (These values were taken from impact studies made in Airbus).

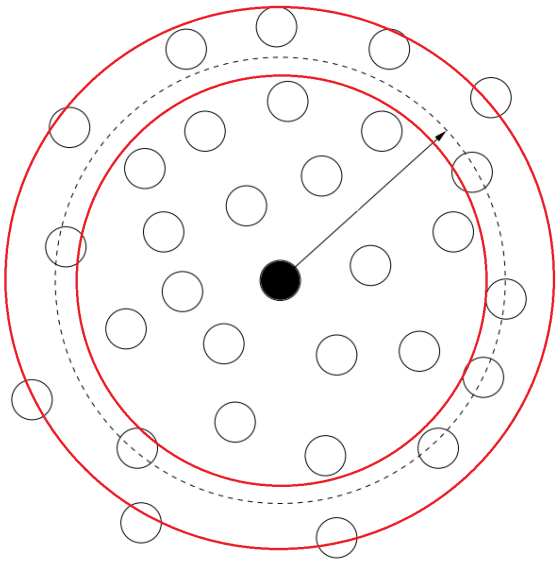

Figure 3.1: Distance of influence of a SPH particle (black line) and the compression and expansion distance (red)

3.3 Introduction to EXPLICIT FEM technique

In Chapter 1 and 2, the analysis of the equations of motion was implicit. This means that equations that are solved are in matrix form and have the form of equation 1.1 or if they can be reduced to modal form, equation 1.9. Differential equations like those are lineal and very stable, which means that the step time (Δt) that has to be used can be of the order of $10^{-3}s$. For this reason, long problems can be solved like DTG, continuous turbulence, etc (the simulation time of these calculations can be of the order of 1-3 min).

For this chapter, non-linear terms are added to the calculations and make it impossible to reduce the equations to matrix form. The evolution of each degree of freedom (d.o.f.) has to be calculated at a time. Moreover, modal form cannot be achieved, so physical coordinates (x, y, z) have to be used. The usual Δt that explicit FEM technique uses is in the order of $10^{-6}s$ which makes the calculations slower than implicit method. Problems like impacts use this explicit techniques and the usual simulation time is around 2-3 seconds.

3.4 Description of the FEM model and fuel sloshing virtual test

In order to build a virtual test, two aspects have to be covered:

- Model: The specimen, how to introduce SPH particles and the configurations that are going to be tested.
- Test description: How the specimen is going to be tested and how the data is going to be extracted.

3.4.1 Model

The model in Pam-Crash is created with PATRAN, the visual interface and pre- and post-processing tool of NASTRAN. Then, it was imported to Pam-Crash, because it can deal with SPHs. This model has the following characteristics:

1. Model length is $10m$, as the previous model.
2. It is a panels model. The model used in Chapter 2 was created with lumped masses and sticks.
3. $20mm$ ribs are introduced in the model as can be seen in Figure 3.2. Ribs were introduced because the model has an upper and a lower skin which have a low buckling frequency. This buckling could affect the subject of the project, which

is the interaction between the liquid and the structure. Although ribs are introduced, the first bending mode frequency is still around $2.5Hz$ and the modal shape is the same as in the A400M wing.

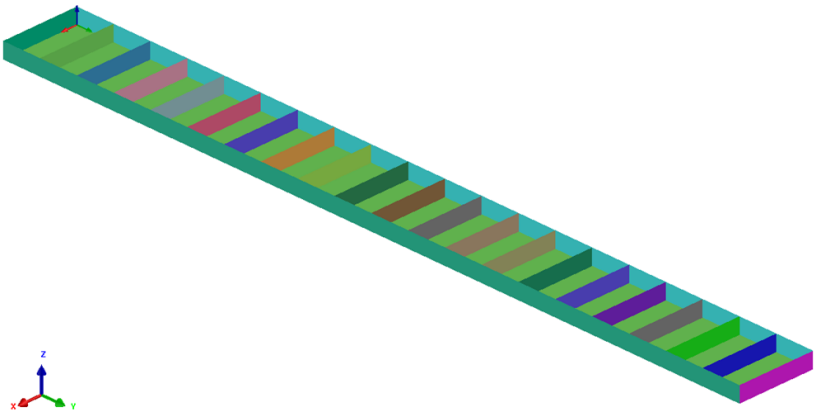

Figure 3.2: 3D Pam-Crash model.

4. Model cross section is the same as in Figure 2.2 except for the thickness. The thickness of the model created for this section is increased to $20mm$. The reason this change is implemented is that the structure deforms plastically when subjected to large displacements ($1m$ tip displacement) and this behaviour was not desirable. Since the thickness is increased, the frequency varies, but the change is minimum (less that 1%).

5. SPH particles are introduced in the model as uniform layers that cover the surface of the lower skin. Each layer contains $16,000$ SPH particles. An example of the 25% and 75% fuel quantity is presented in Figure 3.3.

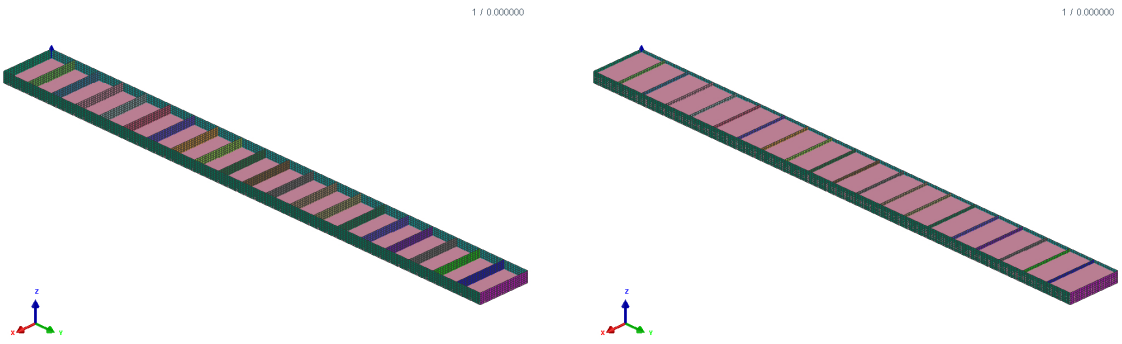

Figure 3.3: 25% of fuel (left) and 75% of fuel (right). Pink layers are made of SPHs.

A closer view of the SPHs is presented in Figure 3.4, where a 25% of particles are represented (2 layers).

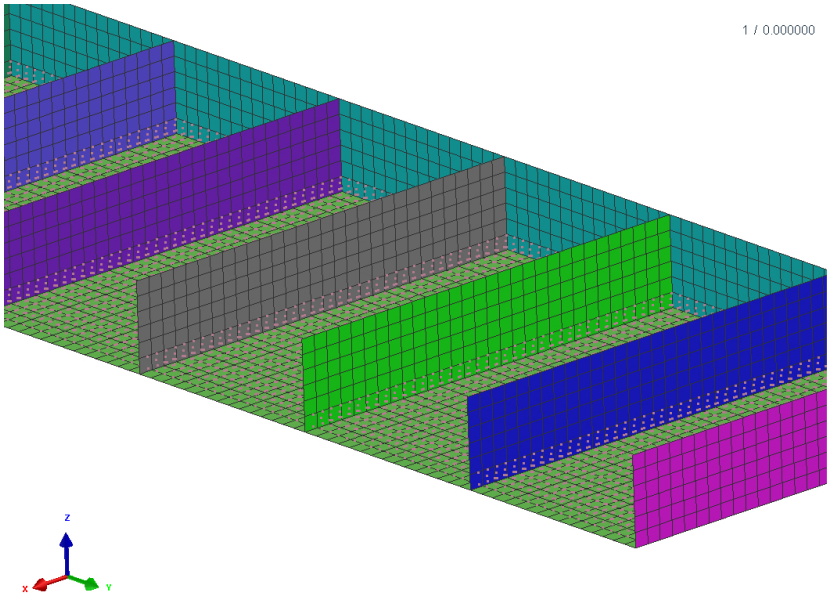

Figure 3.4: Visualization of SPHs. Each pink dot is the representation of a SPH particle.

Configurations of the model

Four model configurations are going to be tested, these configurations introduce modifications on the interaction between SPH particles and ribs:

1. Transparent ribs model. Fuel can pass through interior ribs. This means that SPH particles ignore ribs so they can go through them loosely. The only surfaces that SPH particles are contacting with are front and rear spars, top and bottom skins and first and last ribs (the fuel is confined within the beam). Interior ribs are still helping that the buckling of the surfaces does not occur.

2. Opaque ribs model. Fuel is confined in each bay between ribs. SPH particles contact with every surface and every rib.

3. Small holes model. Fuel can pass through five small holes ($6.67cm \times 6.67cm$) made in interior ribs. Structural characteristics of the model are maintained. It is done through the "contact surfaces" option commented in Section 3.2. For the SPH particles, pink panels in Figure 3.5 do not exist and green ones do.

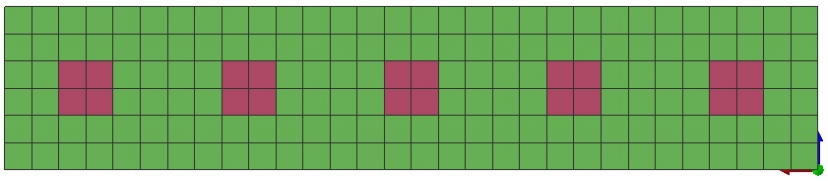

Figure 3.5: Small holes configuration. SPH particles cannot cross green panels but can cross pink ones.

4. Big holes model. Fuel can pass through five big holes ($13.33cm \times 13.33cm$) made in interior ribs. As the small holes model, structural characteristics of the model are maintained and it is done through the "contact surfaces" option commented in Section 3.2.

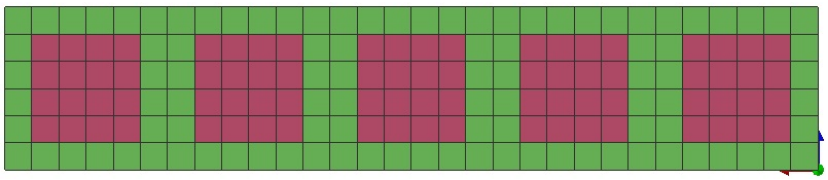

Figure 3.6: Big holes configuration. SPH particles cannot cross green panels but can cross pink ones.

Aircraft ribs in fuel tanks have holes to save weight. To take advantage of these holes, they are used to pass cables, pipes or shafts through them. Since fuel can go through them too, models 3 and 4 were created.

It is important to emphasize that **all the models are structurally identical** and the only difference is from the point of view of the SPH particles.

3.4.2 Test description

The main objectives of this virtual test are the following:

- To be a reference for a physical test.
- To estimate the extra damping that is introduced due to the effect of fuel sloshing.

The virtual test has the following set up:

- As the model in Chapter 2, the beam is clamped at one edge and free at the other one.
- The specimen is subjected to an upward transient force in the tip that follows the profile of Figure 3.7. This profile tries to reproduce a simple physical test: pull

the beam from the edge until certain height and then, suddenly release it. The reason that the applied force is changed is that it is easier to apply the force of Figure 3.7 than a $1 - cos$ force in a real physical test.

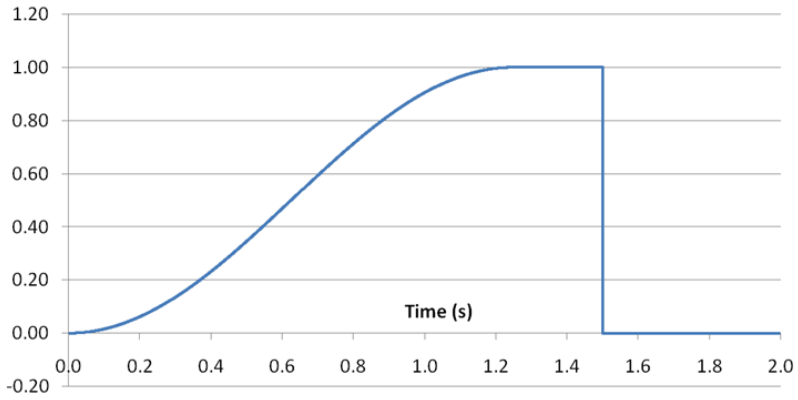

Figure 3.7: Profile of the force.

- Step time was set by Pam-Crash. It is set as the time that the sound takes to cover an element of the structure mesh. The mesh of the structure is been set to elements of $3.33cm$. A finer mesh was tested and the precision was the same and the step time was increased 5 times. Material properties are described in Section 2.2 and sound speed can be calculated with formula 3.1.

$$sound\,speed = \sqrt{\frac{E}{\rho}} = 5164m/s \tag{3.1}$$

  Step time is then around $\frac{3.33cm}{5164m/s} \approx 6{\cdot}10^{-6}s$. With a simulation time of 5 seconds, Pam-Crash takes $3/4h$ to be completed (if SPHs are not added). When SPHs are introduced, simulations can vary between 1 day to 5 days. Since the time for the project is limited, three variations are considered in Chapter 4: fuel quantity, holes in the ribs and displacement of the tip.

- The virtual test is done in absence of gravity, as in Chapter 2.

- The default damping is set to 0%, therefore, if any damping is involved in the response, it will come from the fuel sloshing exclusively.

The desired maximum displacement of the tip could be around 10% of the length of the beam and it is achieved with $100KN$ at the maximum peak, so the force of Figure 3.7 is multiplied by 10^5. This tip displacement is proportional to that of the A400M wing.

In the next Chapter (4), $25KN$, $50KN$, $75KN$ and $100KN$ at the maximum peak will be tested. The model in Chapter 2 was linear, so a higher force would lead to a

proportional response, but, since SPH particles introduce non-linearities, the proportionality is not achieved and the results cannot be predicted.

To prove that NASTRAN and Pam-Crash models are identical, the NASTRAN stick model has been updated with the Pam-Crash model thickness and ribs masses. Then, the force of Figure 3.7 with $100KN$ at its maximum is applied to both of them and the responses are compared in Figure 3.8 which proves that the two models are structurally equivalent.

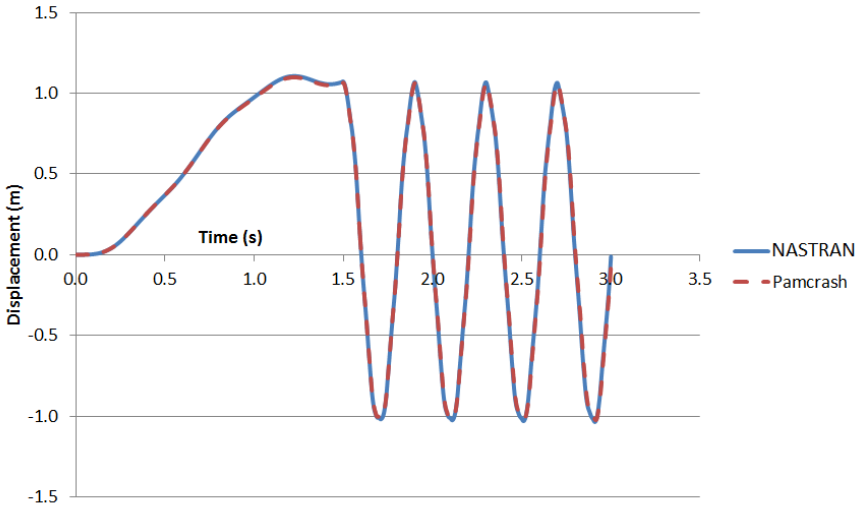

Figure 3.8: Displacement of the tip for a $100KN$ upward force.

Damping extraction

In order to obtain the damping that is being produced by the fuel, logarithmic decrement technique is used. This technique is based in the solution for the equation 1.1 with one degree of freedom:

$$x = Ae^{-\zeta\omega t}sin(\omega t + \gamma) \tag{3.2}$$

where x is the magnitude studied (bending moment, displacement,...), A is a constant, ζ is the ratio of actual damping over critical damping, t is the time, γ is the phase and $\omega = \omega_n\sqrt{1-\zeta^2}$ is the frequency of the system, where ω_n is the undamped natural frequency.

This formula is only valid after the force is released, since it is the solution for an unforced system.

If two peaks of a damped system are selected, the equations are obtained:

$$x_1 = Ae^{-\zeta\omega t_1}sin(\omega t_1 + \gamma) \tag{3.3}$$

$$x_2 = Ae^{-\zeta\omega(t_1+nT)}sin(\omega(t_1 + nT) + \gamma) \tag{3.4}$$

where n is the number of complete oscillations and T is the period of the system. Dividing 3.3 over 3.4, the following equation is obtained since $sin(\omega t_1 + \gamma) = sin(\omega(t_1 + nT) + \gamma)$:

$$\frac{x_1}{x_2} = \frac{\cancel{Ae^{-\zeta\omega t_1}} \cancel{sin(\omega t_1 + \gamma)}}{\cancel{Ae^{-\zeta\omega(t_1+nT)}} \cancel{sin(\omega(t_1 + nT) + \gamma)}} \tag{3.5}$$

Solving for ζ and considering that $\zeta \approx 0$, so $\sqrt{1-\zeta^2} \approx 1$, the logarithmic decrement is solved:

$$\zeta = \frac{1}{\omega n T} ln\left(\frac{x_1}{x_2}\right) = \frac{1}{\omega_n \cancel{\sqrt{1-\zeta^2}}^{\approx 1} nT} ln\left(\frac{x_1}{x_2}\right) = \frac{1}{\cancel{\omega_n} n \frac{2\pi}{\cancel{\omega_n}}} ln\left(\frac{x_1}{x_2}\right) = \frac{1}{2\pi n} ln\left(\frac{x_1}{x_2}\right) \tag{3.6}$$

Equation 3.6 is used in this paper with the first positive peak after the release and the second peak. Then, $n = 1$ and equation 3.6 reduces to 3.7:

$$\zeta = \frac{1}{2\pi} ln\left(\frac{x_1}{x_2}\right) \tag{3.7}$$

This equation is applied to subsequent peaks (second and third, third and fourth,...) and the mean damping is obtained. The results will be commented on Chapter 4.

Chapter 4

Fuel sloshing virtual test results

4.1 Introduction

The results are obtained following this methodology:

1. The beam model is filled with SPH particles.
2. The load is applied at the free tip of the beam model (Figure 4.1, left) and then, the beam is released (Figure 4.1, right) following the profile of Figure 3.7.

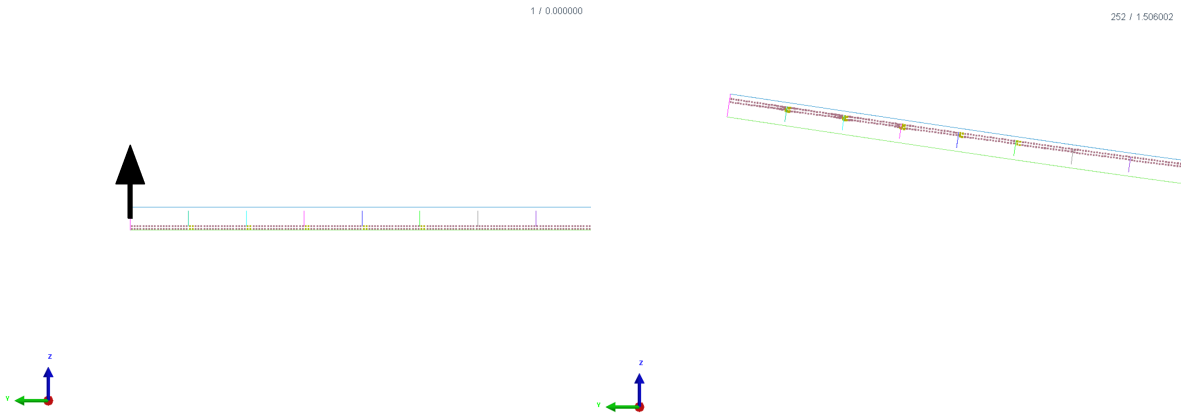

Figure 4.1: $t = 0s$(left) and $t = 1.5s$(right) of the beam with 25% fuel content.

3. The response is compared with the response of the same model without SPH particles.
4. Applying the logarithmic decrement technique (equation 3.7), the mean damping is obtained.

This procedure is kept for all combinations of fuel content and all configurations (see Section 3.4.1).

In Section 4.2, the beam is tested with different fuel contents. The methodology for the damping extraction is presented for the 25% of fuel content as an example.

In Section 4.3, the beam with 25% fuel is tested varying the displacement of the tip.

4.2 Sensitivity to fuel content

For this section and as an example of the procedure, the models that are going to be used are:

- Transparent ribs (see *configurations of the model* in Section 3.4.1)
- Opaque ribs (see *configurations of the model* in Section 3.4.1)

Holes models will be discussed in 4.2.1.

Layers of fuel are added. The more the number of SPHs layers, the more it takes to calculate. Table 4.1 shows the relation between fuel content and CPU time.

Fuel contents	0%	12.5%	25%	50%	75%	100%
SPH layers	0	1	2	4	6	8
CPU time up to T=5s with 6 CPUs	0.7h	6.5h	15.3h	1d 13.7h	2d 19 h	3d 20h

Table 4.1: Fuel content and CPU connection.

Both configurations are loaded at the tip with the force of Figure 3.7 with a peak value of $100KN$. As an example, the beam is filled with 25% of the maximum fuel. For the sake of clarity, displacement of the tip is presented instead of the bending moment in Figure 4.2.

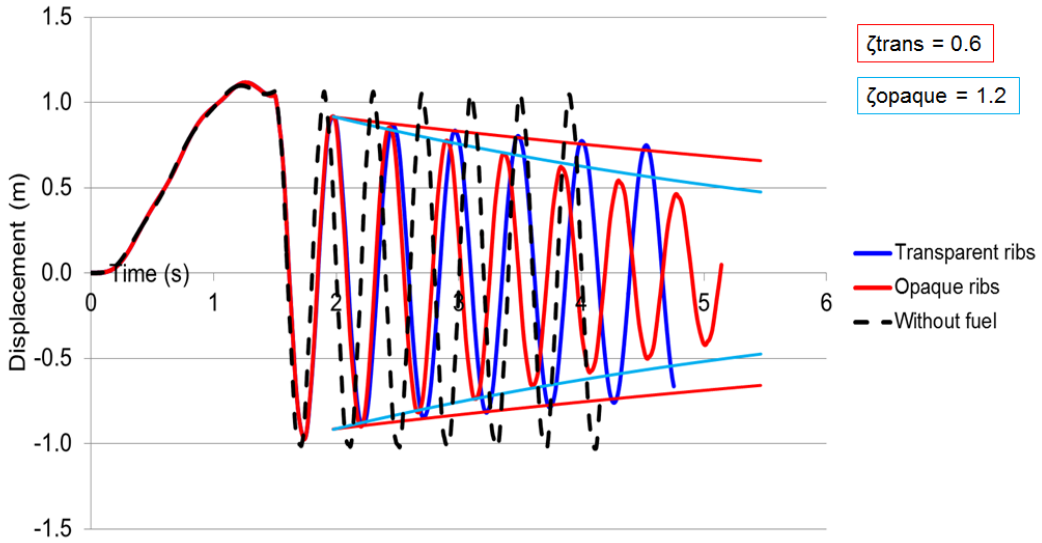

Figure 4.2: Dynamic response of the beam for 25% of fuel content and damping due to fuel sloshing.

Tip displacement damps when fuel is introduced. Part of the kinetic energy of the beam is transferred to the fuel and makes it move. Since the beam is losing energy, the movement becomes gently damped. When the fuel particles hit the beam again, part of the kinetic energy of the fuel is given back to the beam. Energy stored in the fuel particles is the reason of the extra damping.

If fuel can pass through ribs, due to centrifugal force, the fuel goes to the tip. Fuel is accumulated in the tip as can be seen in Figure 4.3 and starts to behave as a concentrated mass and less kinetic energy is transferred. That is why, in the example of Figure 4.2, the damping of the transparent ribs configuration is lower than the opaque ribs one.

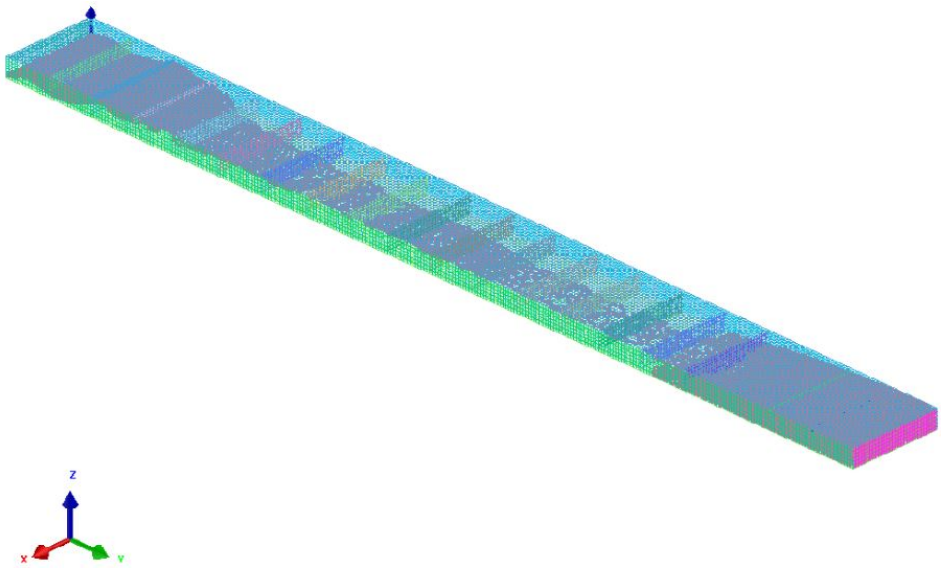

Figure 4.3: Fuel accumulated in the tip at $T = 3.36s$.

On the other hand, if fuel cannot go through ribs, the fuel is confined into their compartments. For the example of 25% fuel content, in each compartment there is 75% of free space where the fuel can move. This movement is not restricted by an accumulation as in the transparent ribs case. For this reason, damping is higher for an opaque configuration.

This test is run for all the fuel content cases and the results for the displacement are shown in Figure 4.4.

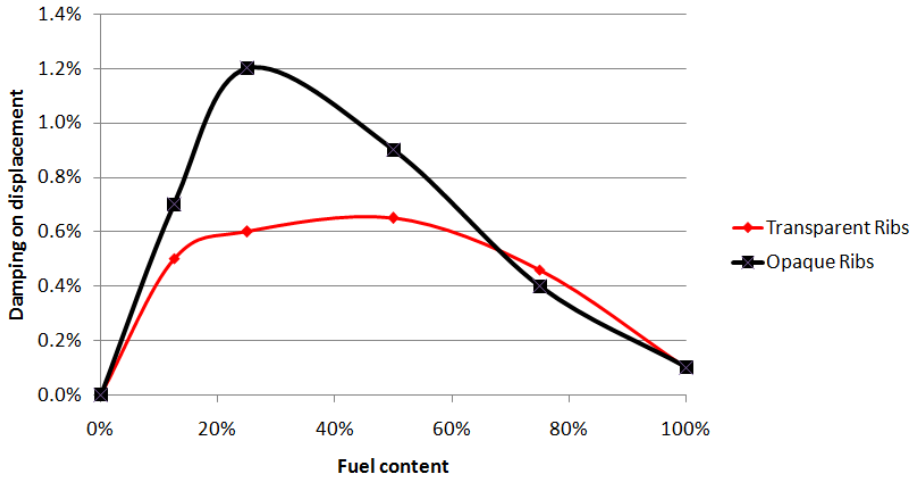

Figure 4.4: Damping on displacement obtained with logarithmic decrement for different fuel contents.

As expected, intermediate fuel contents are the ones where the sloshing effect is larger. A 1.1% of viscous damping in displacement of the tip is estimated with opaque ribs and 25% of fuel content.

Bending moment behaves in a similar way. As can be seen in Figure 4.5, this magnitude is damped a 1.3% due to fuel sloshing with a 25% of fuel content. The difference between damping in displacement and in bending moment is due to dynamic effects.

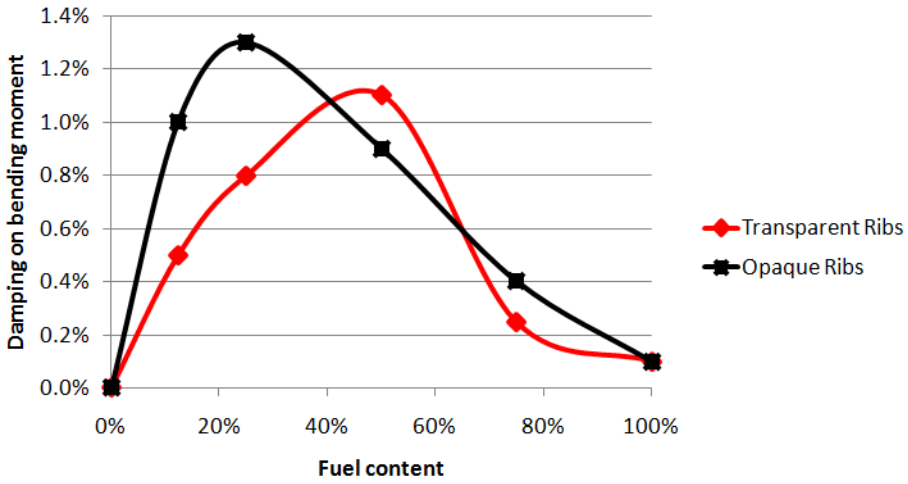

Figure 4.5: Damping on bending moment obtained with logarithmic decrement for different fuel contents.

4.2.1 Sensitivity to different holes in ribs

In this subsection the holes models are studied. When the load is applied and then removed, the fuel tends to go to the tip of the beam due to centrifugal force. However, only a portion of the fuel passes through the next compartment. An example of this transference is shown in Figure 4.6.

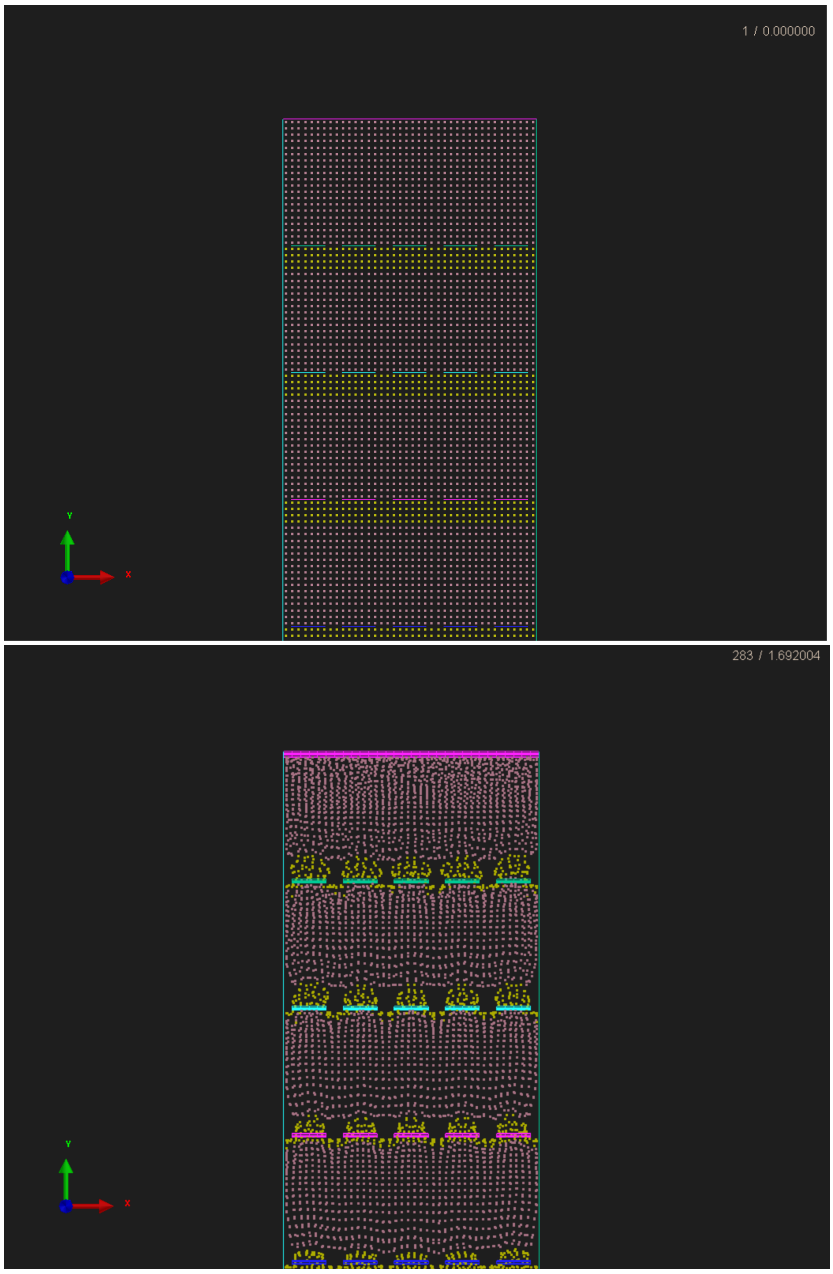

Figure 4.6: Top view of time instant $t = 0s$ (up) and $t = 1.69s$ (down). Some SPH particles has been colored in yellow to help the visualization of the transference.

The responses of these models are in between the transparent and opaque ribs responses. However, contrary to what was expected, "big holes" configuration (which is the most prone to be close to the transparent ribs configuration) barely changes the damping with respect to the opaque configuration as can be seen in Figure 4.7.

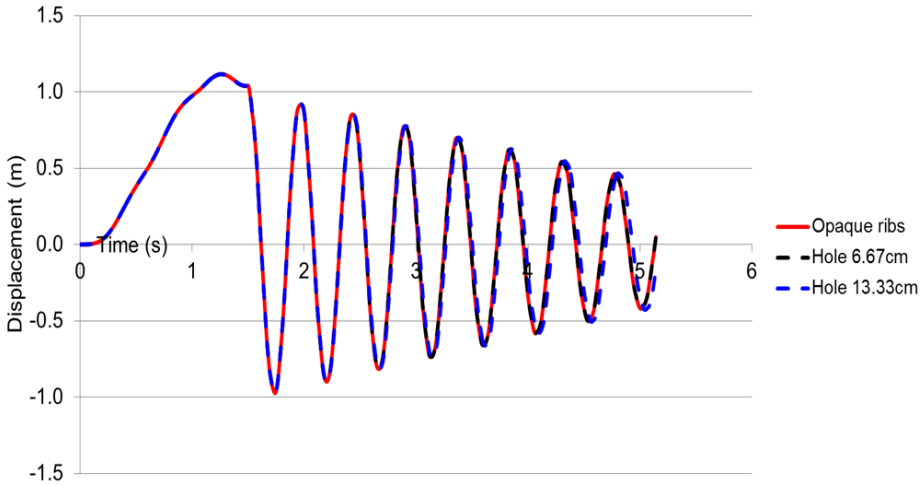

Figure 4.7: Minimum difference on the holes configuration.

Although fuel is traveling towards the tip, it is not enough to see a significant change in the behaviour of the damping. A finer mesh has to be applied in order to make bigger holes and observe the transition between these configurations.

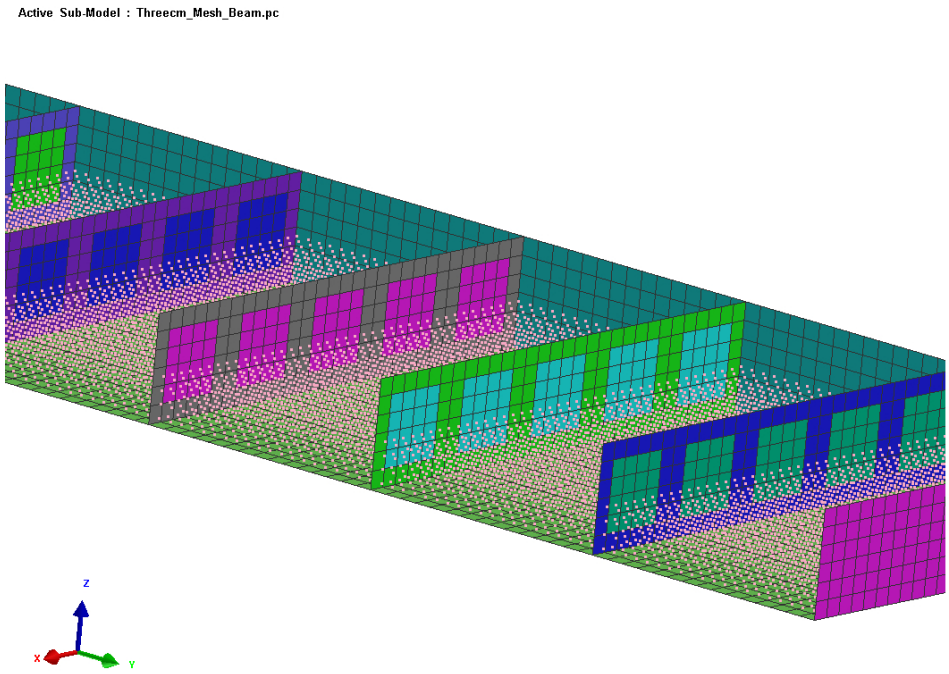

Figure 4.8: Damping does not significantly change from one configuration to another though a lot of particles can move between compartments. Bigger holes could make this change significant.

4.3 Sensitivity to displacement of the tip

Displacement of the tip is an important parameter because it is directly related to the displacement of the fuel. The higher the displacement of the tip, the greater is the movement of the fuel inside the tank.

The critical case (25% fuel content) is studied for $0.25m$, $0.5m$, $0.75m$ and $1m$ tip displacements and the results are the following:

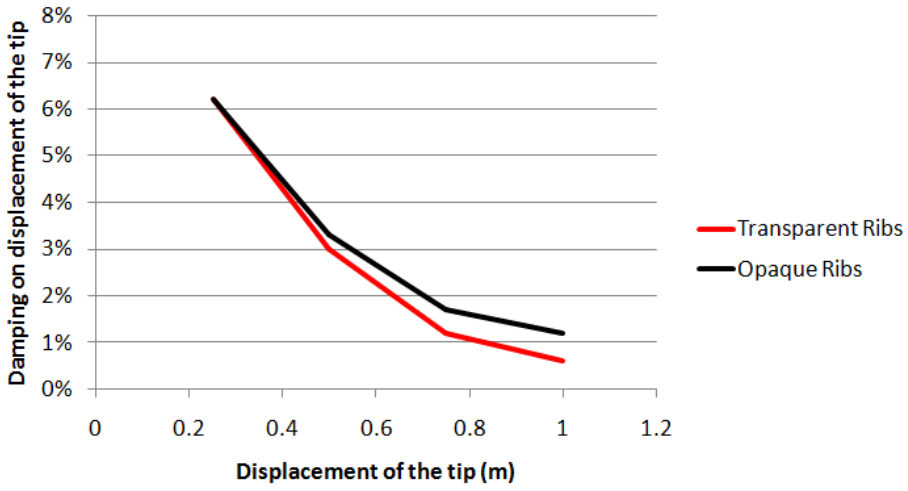

Figure 4.9: Damping on displacement of the tip variation with maximum displacement of the tip.

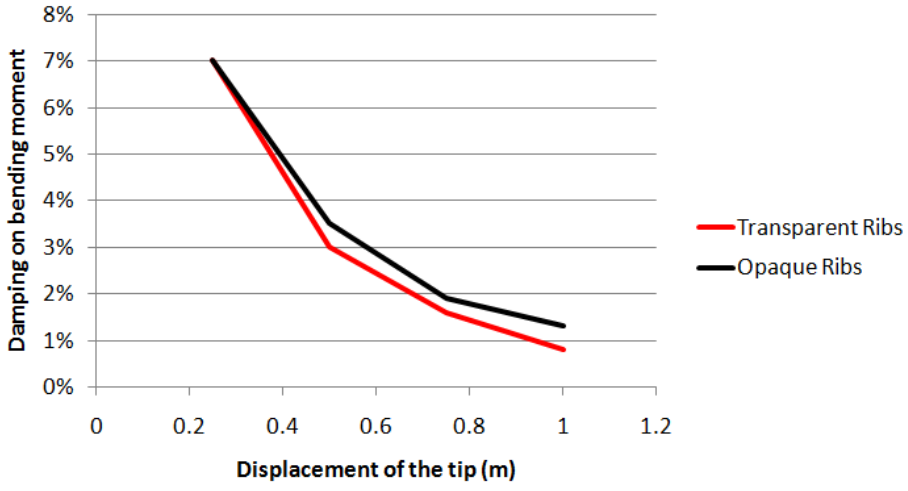

Figure 4.10: Damping on bending moment variation with maximum displacement of the tip.

Contrary to what was expected, the equivalent damping due to fuel sloshing decreases when wing tip displacement increases.

This behaviour could be explained because, when the beam is released at a high tip displacement, the wall that is in contact with the fuel energizes it. As the fuel speeds up, it detaches from the wall, which is slowing down due to the extraction of energy. The fuel moves from one wall to the opposite before the beam has completed half a cycle, that is, when the beam has not yet reached its maximum/minimum for that cycle. While that happens, the fluid follows the wall movement giving back almost all its energy to the wall. As soon as the beam reaches its maximum/minimum, the cycle starts again.

Since SPH particles retain the energy only a few instants, they do not slow down the beam movement. This could be the reason for the low damping when the tip displacement is high.

This fact requires further investigation and will be discussed in Chapter 6.

4.4 Conclusion of the virtual test

Chapter 3 and 4 have shown:

- Extra damping due to fuel sloshing is sufficiently high to be taken into account.
- As expected, intermediate fuel contents are the ones which produce the highest values of extra damping.
- When ribs are introduced, damping effect due to fluid is higher.
- Simulations where fluid is present is very CPU demandant.

Virtual test has demonstrated that a better representation of fluid also helps to damp the response of a dynamic force. Next chapter will propose how to implement this beneficial change into the industry and the expected profits.

Chapter 5

Fuel sloshing modeling proposal and expected dynamic loads reduction

5.1 Introduction

Once the results are extracted from virtual test, original model has to be updated in order to take into account the benefits of fuel sloshing.

Two ways are proposed in this paper:

- Introducing additional damping in NASTRAN. Although the damping that fuel sloshing adds is extracted through the logarithmic decrement technique, in order to validate most models, NASTRAN models must show the same response as Pam-Crash ones.
- Introducing fuel-to-structure connection using springs. Damping in NASTRAN was related to certain springs in Section 2.4, and this could be used in some models in industry. Although the first option is faster to be introduced, this way could be beneficial in other aspects.

The example of 25% fuel content, opaque ribs and $1m$ tip displacement is studied in both models in next sections.

5.2 NASTRAN equivalent damping

NASTRAN model has been used to obtain the equivalent damping that matches the response of Pam-Crash either on root bending moment or in tip displacement. A higher modal damping has to be applied in NASTRAN in most of the cases to match with Pam-Crash, which is even more beneficial to reduce loads.

In Figure 5.1, an example of this adjustment for the displacement is presented.

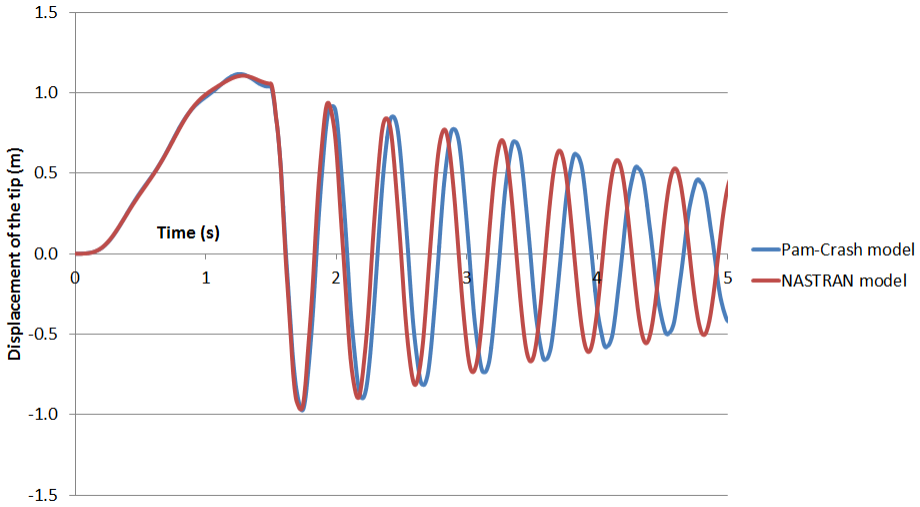

Figure 5.1: Adjustment in displacement for 25% fuel content, opaque ribs configuration and $1m$ max. tip displacement.

Pam-Crash model presents a lower frequency than NASTRAN one because fuel mass is being displaced to the outboard edge of each compartment, and therefore, decreasing the frequency of the system.

This process is repeated for every configuration for the displacement and for the bending moment .The results are presented in Figure 5.2 and 5.3, respectively.

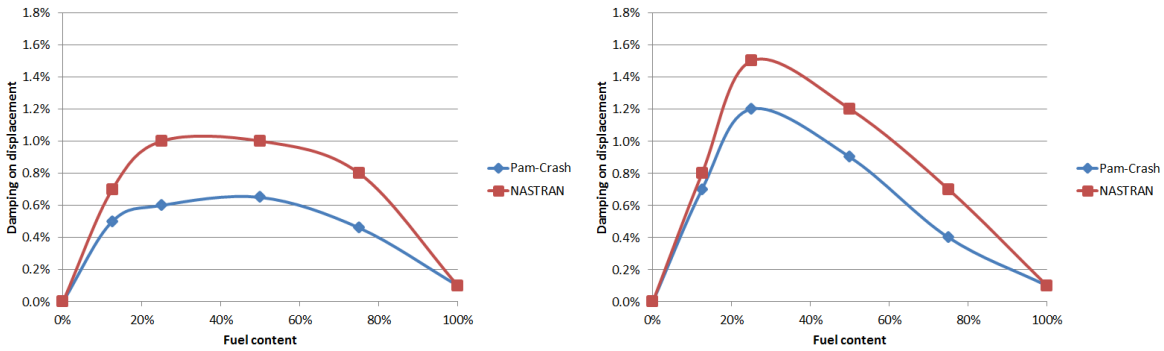

Figure 5.2: Comparison of tip displacement equivalent damping for different fuel contents. Transparent ribs (left) and opaque ribs (right).

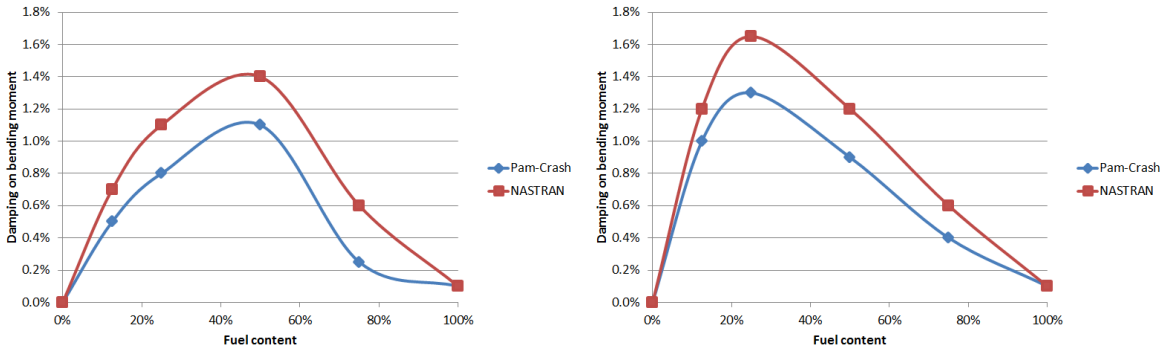

Figure 5.3: Comparison of bending moment equivalent damping for different fuel contents. Transparent ribs (left) and opaque ribs (right).

Bending moment should be damped 1.65% in NASTRAN to obtain the same response than Pam-Crash with 1.3%.

5.3 Fuel-to-structure connection model

For the second way to introduce fuel sloshing, a more particular approach is made. Fuel springs can be connected to elements of the structure instead of applying damping to it.

Once the NASTRAN equivalent damping is obtained, it is correlated thanks to Figures 2.12 and 2.13 as can be seen in Figure 5.4:

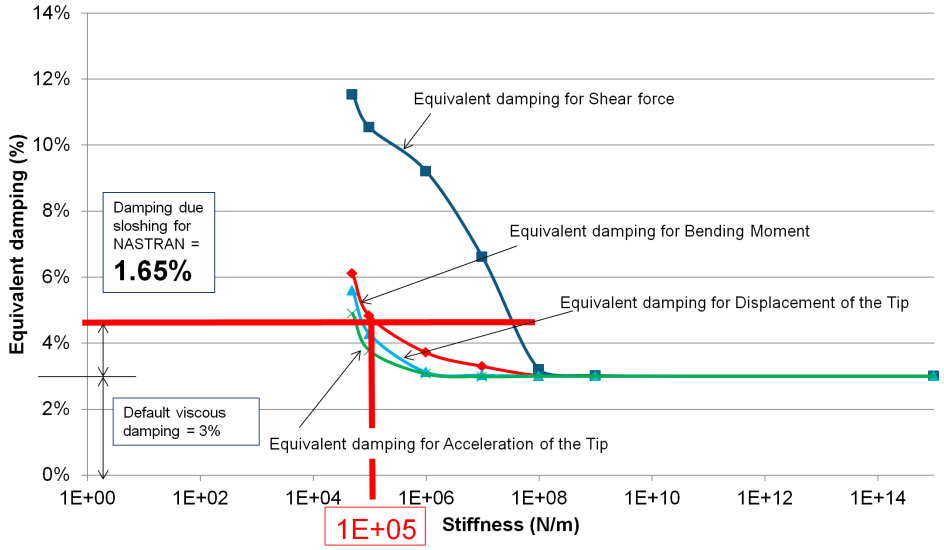

Figure 5.4: Fuel-to-Structure connection stiffness for an equivalent damping.

In order to reproduce the same bending moment as in the example, the stiffness of all the springs have to be set to $10^5 N/m$.

Chapter 6

Future work and Conclusions

6.1 Future work

In order to improve the accuracy of the numerical results, several improvements can be taken into account. This improvements are discussed in Subsection 6.1.1.

A real test should be done to prove that fuel sloshing is indeed helping to reduce dynamic loads. It should be done also to contrast the results obtained in this paper. A conceptual design of this test is presented in Subsection 6.1.2.

6.1.1 Improvements suggested in the numerical simulations

- More holes configuration. The mesh of the Pam-Crash model should be finer in order to be able to connect tests with transparent and opaque ribs configurations.
- Tip displacement. The fact that a lower tip displacement induces a higher damping is contrary to what was expected, so further research must be done.
- Gravity. The study of this paper has been done in absence of gravity. Gravity should be implemented in order to see the changes that are made. This change will increase the CPU time.
- Void force. When the liquid is pushed by the beam in Chapter 4 and then the beam stops moving (it is maintained during $0.25s$), liquid separates from the wall. This is not realistic since there is a vacuum force that retain the particles glued to the beam. This force can be modeled in Pam-Crash with the "separation force" option, which applies an attractive force to the particles that are at a certain distance to the wall. The drawback of this option is that it introduces more non-linearities to the structural model, making it more unstable.
- Different tank geometries. Tests should be made for different tank geometries in order to see what is the effect in a real tank, or bladder tank. Geometry should be an important parameter because liquids do not behave the same in a rectangular tank than in a spherical one.

- Different liquids. Liquid properties are also important since the viscosity and density play an important role in the sloshing.

6.1.2 Real test and estimation of the cost

The best way to test which are the effects of fuel sloshing is to make a real physical test. A beam should be built and filled with liquid (i.e. water) and apply the force of Figure 3.7. These results have to be compared with the ones extracted with this study and adjust the models. A preliminary budget is presented in Table 6.2[1].

Name	Quantity or time	Price	Cost	Description and source
Model support				
Design of the model support	100 engineer hours	42€/h	4,200€	The model support has to be very rigid to withstand high loads barely moving. A conceptual model is presented in Figure 6.1.
Fabrication	2 constructor hours × 100h	20€/h	4,000€	Fabrication of the structure.
Model support transport	-	500€	500€	Since the volume of steel that has to be transported is high, a more expensive transport has been taken into account.
Installation	2 constructor hours × 100h	20€/h	4,000€	Time to clamp the support to the laboratory floor.
Beam model				
20mm thickness aluminum	30m^2	4,834€/m^3	2,900.4€	Square meters of aluminum needed for the making of the model[8].
Rivets	28 boxes of 100 rivets	2.2€/box	61.6€	Needed for fixing the model and make it rigid[9].
Fabrication	2 constructor hours × 50h	20€/h	2,000€	Fabrication of the model.
Model transport	-	300€	300€	Truck that can transport a 10m specimen

[1]NOTE: Prices, costs and times are estimations. June 2014

Name	Quantity or time	Price	Cost	Description and source
Installation in the laboratory	2 constructor hours × 100 h	20€/h	4,000€	Once the model support is installed, the model can be clamped to it.
Measurement system and actuators				
Accelerometers	10 units	150€/unit	1,500€	An accelerometer is placed each meter of beam.
Accelerometers calibration	1 engineer hour per unit	42€/h	420€	It is needed one hour to calibrate each accelerometer.
Wheatstone bridge	4 bridges (4 sensors per bridge)	10€/sensor	160€	In order to obtain the bending moment, shear force and torsor moment in certain points of the model (4 points are enough). A Wheatstone bridge is made out of 4 sensors[10].
Sensors calibration	20 engineer hours per 4 sensors	42€/h	3,360€	20 hours are needed to calibrate a group of 4 sensors.
Actuator	1	2,000€	2,000€	Actuator in order to apply the load needed. A quick release device is also needed
Quick release device	1	500€	500€	Device which releases the load in the actuator without any damage to it. A sudden release can be destructive for the actuator.
Test				
Engineers	4 × 250h	42€/h	42,000€	An estimation of the hours that 4 engineers would spend testing all the configurations.
Laboratory	250h ≈ 1 month	350€/day	10,500€	Place to work.
Water	$10m^3$	$1.458€/m^3$	14.58€	Enough water to fill the beam 10 times[11].

Name	Quantity or time	Price	Cost	Description and source
Pump and drain devices	-	200€	200€	Mechanism to fill the beam with water and drain it for the test.
		$\sum$	**82,616.58€**	

Table 6.2: Preliminary budget for the construction of a real physical test.

A support structure has to withstand the beam model and it has to provide the clamped condition. This means that the structure must not move, so a very stiff support has to be built. Figure 6.1 shows a concept of this structure. On the left hand side of the structure, the beam is clamped. On the right hand side, the actuator applies the load to the tip of the structure.

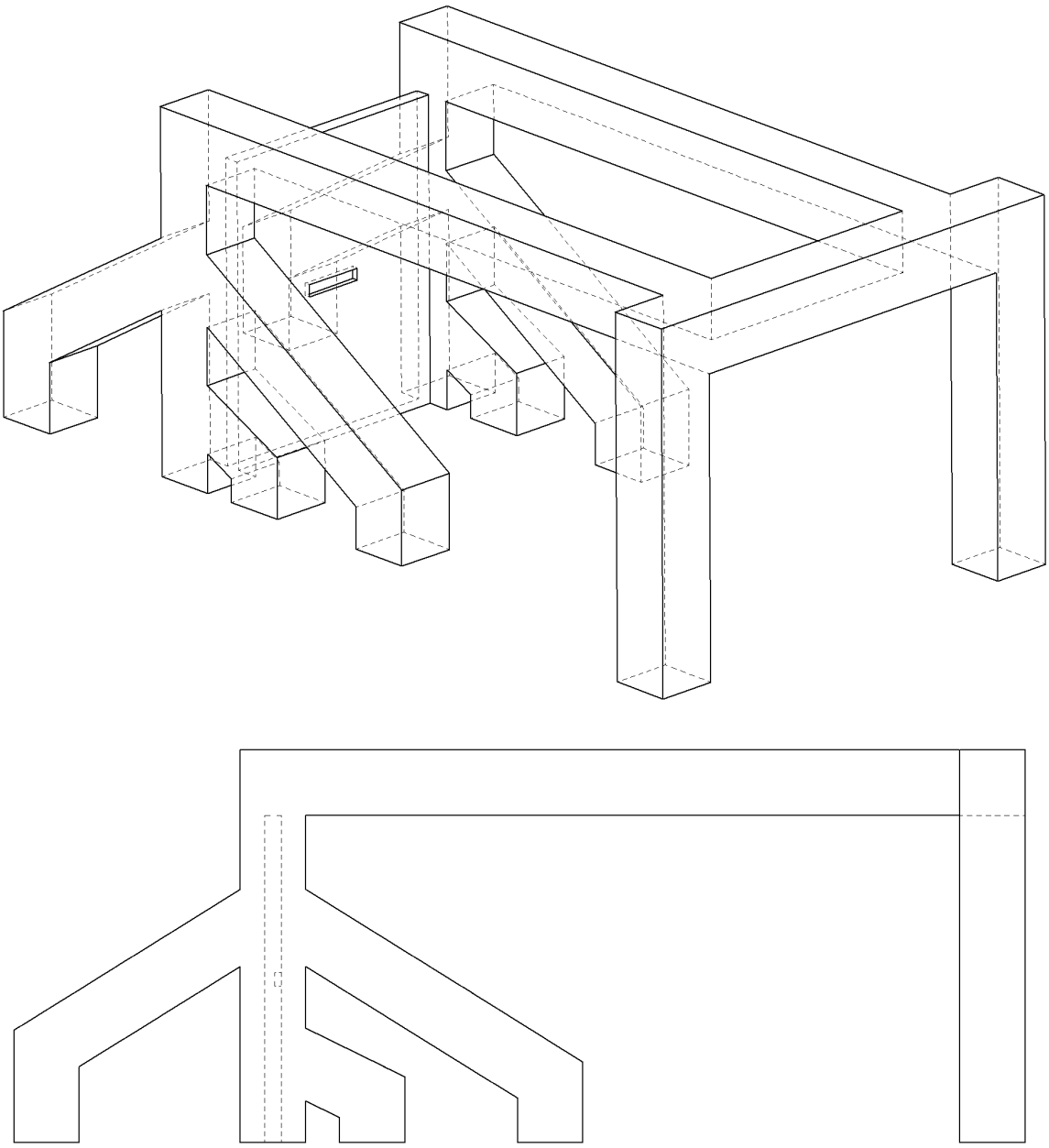

Figure 6.1: Concept of the model support structure.

Concerning the model, an easy way to introduce the ribs configurations must be built. Since the stiffness of the model has to be the same for all configurations, a covering of a stiffer material is used as can be seen in Figure 6.2 modeling the stiffness of the ribs. Grooves are made in the material in order to introduce the ribs. This way, the ribs do not contribute to the stiffness of the system but to the containment of the water.

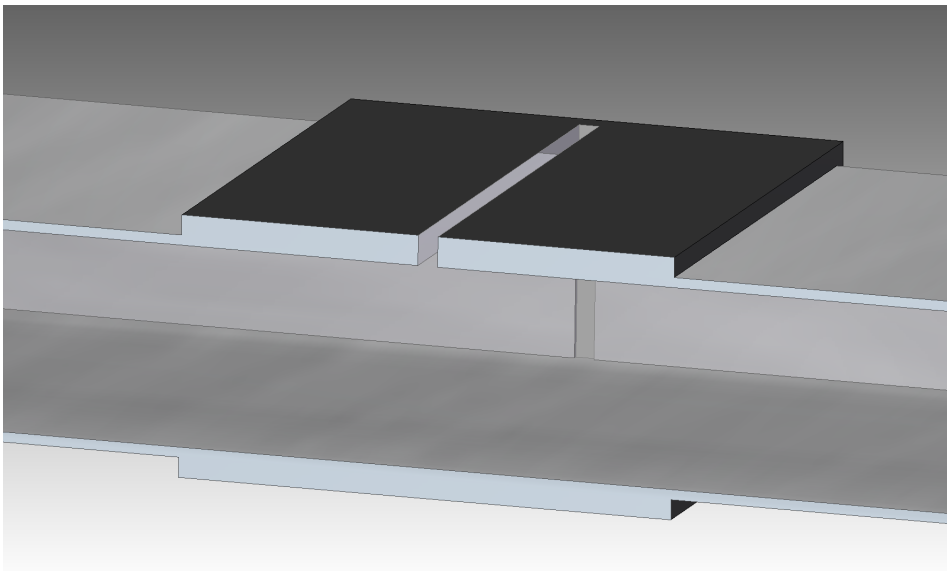

Figure 6.2: Rib stiffness modelization (The model has been cut to see the different parts). Black part is stiffer than aluminum.

Engineers must calibrate each measurement device with known applied forces (empty beam). For the test, every run must be done 3 times at least to ensure the repeatability of the experiment.

6.2 Summary

Fuel sloshing has been proved to be a difficult phenomenon to take into account in industry calculations. However, a simple model can demonstrate that this phenomenon is beneficial to reduce dynamic loads that are critical for the sizing of the aircraft.

Using a real aircraft model (A400M), intermediate fuel content configurations have proven to be the critical ones in certain dynamic loads scenarios. They are also the ones that are prone to have a higher fuel sloshing.

Industry uses a "frozen fuel" model because a realistic fuel model is, nowadays, unaffordable to implement in the industry. Therefore, a simpler model has to be used. This model has demonstrated that a more realistic model of fuel (fuel-to-structure springs) slightly reduces the dynamic loads that the structure has to withstand.

A different technique (SPH) has been used to represent better the fuel behaviour and the results confirmed what was expected in terms of reduction of dynamic loads.

A medium size aircraft can save up around $100kg$ **of wing structure, which means that an additional passenger, paratrooper or more cargo can be inside the aircraft. A commercial aircraft with** $25,000$ **life cycles which implements this improvement could make** $\$5,000,000$ **more than the same aircraft without this consideration (**$\$200/ticket$**).**

Bibliography

[1] Firouz-Abadi R. D., Haddadpour H., and Ghasemi M. A boundary element method for investigation of sloshing in complex 3d containers. In *48th AIAA/ASME/ASCE/AHS/ASC Structures, Structural Dynamics, and Materials Conference*, 2007.

[2] Ibrahim R. A. *Liquid sloshing dynamics: theory and applications*. Cambridge University Press, 2005.

[3] Thelander J. A. Aircraft motion analysis. Technical report, DTIC Document, 1965.

[4] Chatman Y., Gangadharan S., Schlee K., Sudermann J., Walker C., Ristow J., and Hubert C. Mechanical analog approach to parameter estimation of lateral spacecraft fuel slosh. 2007.

[5] Monaghan J. J. Smoothed particle hydrodynamics. *Annual review of astronomy and astrophysics*, 30:543–574, 1992.

[6] Banim R., Lamb R., and Bergeon M. Smoothed particle hydrodynamics simulation of fuel tank sloshing.

[7] Climent H., Viana J.T, Benitez Montañes L., Pérez Muñoz J.D., and Kamoulakos A. *Advanced Simulation (using SPH) of Bird Splitting, Ditching Loads and Fuel Sloshing*. Proceedings of the ESI Global Forum 2014, Paris, France 21-22 May 2014.

[8] *http://spanish.alibaba.com/product-gs/20mm-thick-aluminium-sheet-hot-rolled-aluminium-plate-5052-688508645.html?s=p*.

[9] *http://www.sodimac.cl/sodimac-cl/product/233285/Remache-Pop-4,8-x-18-100-unidades?color=&passedNavAction=push*.

[10] *http://en.wikipedia.org/wiki/Wheatstone_ bridge*.

[11] *http://www.canalgestion.es/es/galeria_ficheros/comunicacion/publicaciones/Tarifas_ 2014.pdf*.

List of Figures

List of Tables